

Evaluating the Generalization Ability of Super-Resolution Networks

Yihao Liu^{1,2,3}, Hengyuan Zhao^{1,5}, Jinjin Gu^{3,4}, Yu Qiao^{1,3}, and Chao Dong^{1,3}

¹ Shenzhen Institute of Advanced Technology, CAS

² University of Chinese Academy of Sciences ³ Shanghai AI Laboratory

⁴ The University of Sydney ⁵ National University of Singapore

liuyihao14@mails.ucas.ac.cn, hengyuan.z@u.nus.edu,
jinjin.gu@sydney.edu.au, {yu.qiao, chao.dong}@siat.ac.cn

Abstract. Performance and generalization ability are two important aspects to evaluate deep learning models. However, research on the generalization ability of Super-Resolution (SR) networks is currently absent. We make the first attempt to propose a **Generalization Assessment Index** for SR networks, namely SRGA. SRGA exploits the statistical characteristics of internal features of deep networks, not output images to measure the generalization ability. Specially, it is a non-parametric and non-learning metric. To better validate our method, we collect a patch-based image evaluation set (PIES) that includes both synthetic and real-world images, covering a wide range of degradations. With SRGA and PIES dataset, we benchmark existing SR models on the generalization ability. This work could lay the foundation for future research on model generalization in low-level vision.

1 Introduction

Deep learning has achieved great success in constrained environment, and we have steadily moved our attention to its generalization ability. Generalization determines whether an algorithm can work well on unseen data. However, due to the data-driven nature, deep learning can easily overfit the training data, resulting in an unpredictable generalization behavior. In this work, we will discuss the problem of generalization in the regime of image super-resolution (SR), which is a classic low-level vision problem. Conventional SR models are generally trained under known degradation types and downsampling kernels, thus their performance deteriorates severely in real-world images [6,15,35]. How to improve the generalization ability is of great importance for developing future methods.

The problem of super-resolving images with unknown degradations is also called blind SR or real SR. Existing methods can be categorized into four classes, including degradation specific methods [37,47], kernel estimation methods [6,15], unsupervised methods [44,16] and internal statistical methods [31,1], which are detailed in a blind SR survey [13]. Remarkably, recent works based on synthetic data have made significant progress. For example, BSRGAN [47] and

Real-ESRGAN [37] show that when we can synthesize enough degradations, the model can be applied in a wide range of real-world scenarios. This phenomenon is also observed in blind face restoration task, like GFP-GAN [36] and G PEN [43]. They all show impressive results on some real-world images. Recently, [10] introduces Dropout [32] to improve the generalization of SR networks.

However, there comes the problem: how to measure their generalization ability? We may also wonder: what are the failure cases and whether increasing the degradation types is a correct direction? All these require us to objectively evaluate the generalization ability. Existing works can only show some visual examples, but do not provide any feasible evaluation strategies. Without a standard evaluation metric and dataset, we cannot fairly compare different models, restricting the progress of their development.

However, the evaluation of generalization is by no means easy! There is no specific assessment for generalization ability. In high-level vision tasks, like classification, they usually use the prediction accuracy on an unseen dataset or category as the generalization measure [9,46,26,25,27]. But in low-level vision tasks, like image restoration, there are no appropriate strategies. Can we use image quality assessment (IQA), such as PSNR and NIQE[20], to take the place of generalization assessment (GA)? The answer is NO, and there are three main reasons. First, IQA is designed to evaluate the image quality, yet image quality is not equal to generalization ability. For example, traditional interpolation or filtering methods get lower IQA values than deep models in most cases, but they have a stable performance (good generalization ability) on all kinds of data. Generalization should be a relative notion that is correlated with the method itself, not only the output. Second, IQA is highly sensitive to image content, thus will have different values on different images. While in image restoration, we need to give a stable measurement on unseen degradations but not specific datasets. Third, IQA itself is not perfect. The reference-based IQA, like PSNR and SSIM, cannot be used in real-world images without ground truth, while the non-reference IQA, like NIQE and PI [3], cannot accurately evaluate the image quality. Gu et.al [5] have proved that existing IQA methods all have low correlation rates with human subjective scores on PIPAL dataset [8]. The above three issues have stopped IQA from being a qualified GA.

To fill in the gap, we make the first attempt to propose a complete evaluation protocol, including a GA index, a series of test datasets, and a benchmark, which could provide a comprehensive evaluation of the generalization ability. Before presenting our method, we clarify the basic definitions of generalization in SR task, and provide some general principles for the new index design. Afterwards, we propose the first Generalization Assessment index for SR task – SRGA. SRGA is based on the statistical characteristics of internal features of the model, not output images. It is calculated on the test dataset, but is not sensitive to the data selection. More interestingly, it is a non-parametric and non-learning metric, which is guaranteed to have a good generalization ability itself. To better validate our method, we collect a patch-based image evaluation set (PIES) that includes both synthetic data and real-world images, covering

a wide range of degradations. On this basis, we can benchmark existing SR models on generalization ability. The benchmarking results are mostly consistent with our common sense. For instance, BSRGAN and Real-ESRGAN have a good generalization performance on most datasets, and are superior to other blind SR methods. We also have some surprising discoveries, like SwinIR [12] generalizes better on heavier noisy degradation, which could provide further insights on these methods. We hope our SRGA and datasets can help promote the development of blind SR methods, as well as other low-level vision problems.

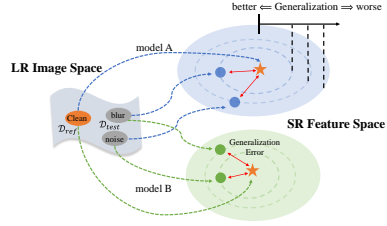


Fig. 1. Illustration of measuring the generalization ability in model internal feature space.

Methods	Clean	Blur1	Blur2	Blur4
SRResNet	$\underline{\sigma}$ 2.718	2.532	2.333	2.083
(train: clean)	$\underline{\alpha}$ 0.687	0.661	0.596	0.494
SRResNet	$\underline{\sigma}$ 2.866	2.783	2.795	2.465
(train: blur0-4)	$\underline{\alpha}$ 0.691	0.682	0.683	0.591
SwinIR-GAN	$\underline{\sigma}$ 5.178	5.140	5.069	4.929
	$\underline{\alpha}$ 0.740	0.742	0.742	0.733

Table 1. The estimated GGD parameters of representative methods with different degraded input.

2 Preliminaries

How to measure the generalization ability in SR task? Generally, we use the generalization error to measure the generalization ability [24,49]. The generalization error is easy to define in high-level vision tasks, which can be calculated by the distance between ground-truth (GT) labels and the model predictions. However, in low-level vision, there are no GT images in most cases, and one input image can correspond to multiple GT images, due to the ill-posed nature. It is hard to directly measure the restoration accuracy. It is acknowledged that deep model could achieve the best performance on in-distribution data (same distribution as the training data), but can hardly generalize to out-distribution data (different distribution as the training data). Thus, it is reasonable to define the generalization error in SR as the performance gap between the in-distribution and out-distribution data. As shown in Fig. 1, the in-/out-distribution inputs are distributed in two separate image spaces. After processing, they are expected to lie in the same space, indicating a better generalization ability. The gap between these two output spaces is the generalization error, and GA index is exactly the measurement of such a generalization error.

What are the general principles for GA design? From the above descriptions, we can summarize four unique characteristics of GA and introduce the corresponding design principles. (1) GA index should be correlated with both the model and the test data. Thus, it is better to take advantage of the model, not only the output image. (2) GA index should be a relative measure that calculates the distance between the reference (e.g., in-distribution data) and the test data (e.g., out-distribution data). Thus, it is essential to determine the reference data beforehand. (3) GA index in low-level vision should be sen-

sitive to degradation, but insensitive to image content. Thus, it is important to disentangle image degradation from content. (4) GA index should have good generalization ability itself. Thus, it is preferable to devise a non-learning (not rely on training data) and non-parametric (not rely on human setting) metric.

3 Formulation

Model Performance. Given a trained SR model G and a set of test input images $S_{\mathcal{D}} = \{I_n\}_{n=1}^N$ with degradation \mathcal{D} , the predicted SR results are obtained by: $I_n^{SR} = G(I_n)$. To evaluate the performance of model G , we can quantify the distance between the predicted output and the ground truth (GT) image I_n^{HR} :

$$Perf(G, S_{\mathcal{D}}) = \sum_{n=1}^N Dist(I_n^{SR}, I_n^{HR}), \quad (1)$$

where $Dist(.,.)$ is a distance or similarity function, such as L_2 error, PSNR, SSIM [40], LPIPS [48] or other image quality evaluation metrics. The Equ. (1) describes the average performance of model G on the test set $S_{\mathcal{D}}$. Note that the model performance is actually affected by image content and degradation simultaneously. That is, datasets with the same degradation but different image content will result in different performance scores.

Model Generalization Ability. Unlike model performance, model generalization ability should characterize the consistency of the model's processing effects across different types of input data, rather than absolute performance values. A model with good generalization ability should have similar processing effects for different types of inputs.

Formally, given two different input sets $S_{\mathcal{D}_1}$ and $S_{\mathcal{D}_2}$, model generalization measures the difference between the processing effects of G on $S_{\mathcal{D}_1}$ and $S_{\mathcal{D}_2}$:

$$Gen(G, S_{\mathcal{D}_1}, S_{\mathcal{D}_2}) = Dist(\mathcal{F}(G, S_{\mathcal{D}_1}), \mathcal{F}(G, S_{\mathcal{D}_2})), \quad (2)$$

where $\mathcal{F}(G, S_{\mathcal{D}})$ is a function that represents the processing effect of model G on dataset $S_{\mathcal{D}}$. It should concentrate more on the image degradation \mathcal{D} instead of image content. In this paper, we explore the intrinsic statistics of deep features of SR networks, and propose a statistical modeling for evaluating the model generalization ability.

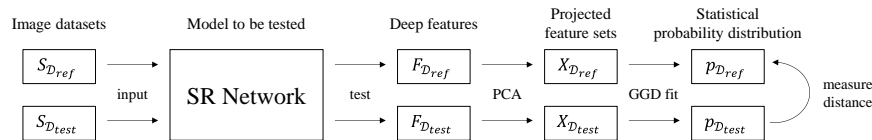


Fig. 2. Schematic pipeline for calculating the proposed generalization index SRGA.

4 Statistical Modeling of Deep SR Networks

4.1 Overview of the Proposed SRGA

The overview of the proposed generalization ability metric SRGA is depicted in Fig. 2. SRGA is built upon the statistical modeling of deep features of SR networks. It is a relative measurement that computes the distance of the feature distributions between the in-distribution reference dataset and the candidate test dataset. Note that the reference dataset is the one that the model can well perform on, which is usually within the training distribution. We first obtain the corresponding deep features of the input datasets. Then, the features are compressed by principal component analysis (PCA), after which we adopt generalized Gaussian distribution to model the projected features sets. Finally, the generalization error is measured by the Kullback-Leibler divergence (KLD) between the two probability distributions, leading to the proposed generalization index SRGA. In the following, we will elaborate on the details of the adopted statistical methodology.

4.2 Revisit Natural Image Statistics

For decades, lots of efforts have been made to explore the statistics of natural images [28,29,34,21]. For example, Mallat [17] discovered that coefficients of multi-scale and orthonormal wavelet decompositions of images could be described by the generalized Gaussian model. Moulin and Liu [22] analyzed the multi-resolution (wavelet) image denoising schemes using generalized Gaussian and complexity priors. Among these works, Mittal *et al.* [19] discovered that the image mean subtracted contrast normalized (MSCN) coefficients in the spatial domain have characteristic statistical properties that are strongly correlated to the image distortion. They adopted the generalized Gaussian distribution to model the MSCN coefficients, and successfully proposed the widely-used no-reference image quality assessment (NR-IQA) BRISQUE [19] and NIQE [20]. A recent work [14] further discovered the deep degradation representations (DDR) hidden in the SR networks: the deep features of SR networks are spontaneously discriminative to image degradations rather than image contents.

Inspired by these researches, we present a new perspective for studying the generalization ability of deep models. Specifically, we explore the statistics of deep features of SR networks and successfully build a statistical model to quantitatively measure the generalization ability.

4.3 Statistics of Deep Features of SR Networks

Given a set of N input images $\{I_n\}_{n=1}^N$ with degradation \mathcal{D} , for arbitrary super-resolution model G , we can obtain its corresponding deep features $\{F_n\} = \{G_F(I_n)\}$, where $F_n \in \mathbb{R}^{H \times W \times C}$, H , W and C are the height, width and depth, respectively. G_F denotes the model containing all the layers before the last output layer, *i.e.*, F_n is the extracted deepest feature map before the output layer. More details are described in the supplementary file.

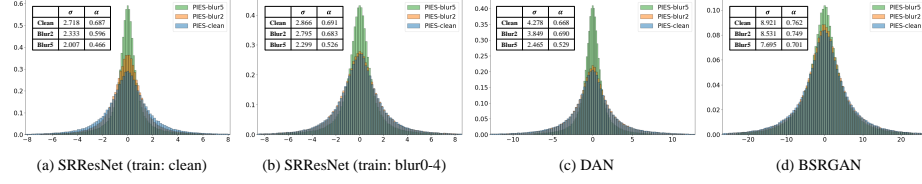


Fig. 3. Statistics of deep features of SR networks. Different distributions will lead to different parameters. The distribution differences within the training data (well generalized region) are usually small, while the distribution outside the training data deviates significantly. This potentially reveals the difference of the processing effects for various degradations. By measuring the distribution differences, we can approximately evaluate the model generalization ability.

Firstly, we apply PCA [41] to reduce the dimension of $\text{vec}(F_n)$ ¹ from HWC to D , to alleviate the calculation cost and compress information.² Specifically, $Y = [\text{vec}(F_1); \text{vec}(F_2); \dots; \text{vec}(F_N)] \in \mathbb{R}^{N \times HWC}$. The PCA method will find a projection matrix $P \in \mathbb{R}^{HWC \times D}$, resulting in $X = YP, X \in \mathbb{R}^{N \times D}$. Denote $\text{set}(X) = \{X(j, k) | j \in \{1, 2, \dots, N\}, k \in \{1, 2, \dots, D\}\}$. The cardinal of $\text{set}(X)$ is $N \times D$. Our finding is that the elements $x \in \text{set}(X)$ have the statistical properties that are determined by the model G and the degradation type \mathcal{D} . Formally, x obeys probability distribution $p_{G, \mathcal{D}}$: $x \sim p_{G, \mathcal{D}}(x)$.

In order to visualize how the distributions $p_{G, \mathcal{D}}$ vary as a function of the model G and input degradation \mathcal{D} , Fig. 3 plots the histograms of $x \in \text{set}(X)$ with different G and \mathcal{D} on PIES dataset (described in Sec. 5). From the statistical results, we can draw several important observations: 1) For a given model G , different input degradation types \mathcal{D}_1 and \mathcal{D}_2 will lead to different probability distributions p_{G, \mathcal{D}_1} and p_{G, \mathcal{D}_2} . By quantifying the distance between these two resulting probability distributions, it is possible to measure the difference in the processing effect on different input distributions. 2) For degradation type \mathcal{D} , different model G will produce different distributions, implying that each model has created its own feature manifold, which determines the generalization ability.

4.4 Generalized Gaussian Distribution

To model and analyze the statistics of the deep features of SR networks, we explore to fit the empirical distributions $p_{G, \mathcal{D}}$ with an appropriate statistical distribution. The Generalized Gaussian Distribution (GGD) is widely used for many relevant tasks, since its form is general and covers many common distributions like Gaussian distributions, Laplace distributions and uniform distributions. More importantly, extensive practice has demonstrated that GGD can fit natural image statistics, and the deep features extracted by SR networks inherit such properties. We discover that the statistical properties of deep features are changed by the presence of distortion, and quantifying these changes can

¹ Flatten the spatial feature map into a one-dimensional vector.

² In our experiments, D is set to 300. Other reasonable values (> 300) also work fine.

make it possible to measure the processing effect of the model on different input degradations. The GGD with zero mean is formulated as:

$$GGD(x; \alpha, \sigma^2) = \frac{\alpha}{2\beta\Gamma(1/\alpha)} \exp\left(-\left(\frac{|x|}{\beta}\right)^\alpha\right), \quad (3)$$

where

$$\beta = \sigma \sqrt{\frac{\Gamma(1/\alpha)}{\Gamma(3/\alpha)}}, \quad (4)$$

and $\Gamma(\cdot)$ is the gamma function:

$$\Gamma(z) = \int_0^\infty t^{z-1} e^{-t} dt \quad (z > 0). \quad (5)$$

There are two parameters α and σ in GGD. The parameter α controls the “shape” of the distribution. $\alpha = 1$ and $\alpha = 2$ yield the Laplacian and the Gaussian density function, respectively. Smaller values of the shape parameter lead to more peaked distributions. Another parameter σ controls the variance. Intuitively, the natural image contents are presented by the distribution, while the degradation changes the distribution parameters.

We try to match the empirical histograms of the feature sample values $x \in X$ with the best possible GGD pdf. Specifically, we adopt the moment-matching based method proposed in [30] to estimate the parameters α and σ of GGD. Tab. 1 summarizes the statistics of several representative models with different input degraded images. The complete results are in the supplementary materials.

4.5 Measuring Model Generalization Ability

In the previous sections, we have revealed that different input degradation types will lead to different feature distributions. Ideally, if model G is robust enough and has perfect generalization ability, the outputs of different inputs should be of the same distribution or very close to each other. Hence, by quantifying the distance between these two probability distributions, we can measure the difference of processing effects between different input distributions, which reflects the model generalization performance.

In practice, given two sets of input images with different degradation types $\{I_n\}^{\mathcal{D}_1}$ and $\{I_n\}^{\mathcal{D}_2}$, we first obtain their corresponding deep feature sets $\text{set}(X^{\mathcal{D}_1})$ and $\text{set}(X^{\mathcal{D}_2})$. Then, we adopt GGD to fit the datapoints to model the feature statistics: $p_{G, \mathcal{D}_1}(x) = GGD(x; \alpha_1, \sigma_1^2)$, $p_{G, \mathcal{D}_2}(x) = GGD(x; \alpha_2, \sigma_2^2)$. Once the distribution parameters have been estimated with the deep features, we can capture the distribution change by calculating the Kullback-Leibler divergence (KLD) between distributions. Fortunately, the KLD of two zero-mean Generalized Gaussian Distribution $GGD(x; \alpha_1, \sigma_1^2)$ and $GGD(x; \alpha_2, \sigma_2^2)$ has the closed-

form solution [42]:

$$D_{kl} = \ln \frac{\alpha_1 \sigma_2 \Gamma(1/\alpha_2) \sqrt{\Gamma(1/\alpha_2) \Gamma(3/\alpha_1)}}{\alpha_2 \sigma_1 \Gamma(1/\alpha_1) \sqrt{\Gamma(1/\alpha_1) \Gamma(3/\alpha_2)}} + \left(\frac{\sigma_1 \sqrt{\Gamma(1/\alpha_1) \Gamma(3/\alpha_2)}}{\sigma_2 \sqrt{\Gamma(1/\alpha_2) \Gamma(3/\alpha_1)}} \right)^{\alpha_2} \frac{\Gamma(\alpha_2/\alpha_1 + 1/\alpha_1)}{\Gamma(1/\alpha_1)}. \quad (6)$$

Now, we have an analytical approach to quantitatively measure the difference in the output feature distributions caused by different input images. Specifically, to evaluate the generalization ability of model G , a reference dataset $S_{\mathcal{D}_{ref}}$ should be selected (*i.e.* known in-distribution data that the model can perform well), then we compute the feature distribution distance (FDD) between the reference dataset $S_{\mathcal{D}_{ref}}$ and the test dataset $S_{\mathcal{D}_{test}}$:

$$FDD = D_{kl}(P(G, S_{\mathcal{D}_{ref}}), P(G, S_{\mathcal{D}_{test}})), \quad (7)$$

$$SRGA = \log_{10}(FDD + 10^{-\delta}) + \delta, \quad (8)$$

where $P(G, S_{\mathcal{D}})$ represents the generalized Gaussian distribution fitted by the deep features of model G with the input dataset $S_{\mathcal{D}}$. Smaller FDD means that G has similar processing effects on these two different input degradations. δ is introduced to avoid zero point in logarithmic function and the min value is shifted to 0 by adding δ (we set $\delta = 5$). The proposed SRGA is a plausible representation of $Dist$ and \mathcal{F} in Equ. (2). Further, if there are N test datasets $\{S_{\mathcal{D}_{test}}^i\}$, we can calculate the mean value of the SRGA:

$$mSRGA = \frac{1}{N} \sum_i^N SRGA(P(G, S_{\mathcal{D}_{ref}}), P(G, S_{\mathcal{D}_{test}}^i)). \quad (9)$$

Notably, mSRGA describes the averaged generalization ability across multiple degradation datasets. It is actually averaging different **degradations** not the contents of the datasets. For the same degradation but different contents, SRGA is not sensitive; for different degradations, mSRGA can give a mean value. It is worth noting that such a measurement method does not require any paired ground truth (GT) image or even the final output image. Further, even if the contents of the two sets of input images are completely different, we can still measure the difference between them. Because the probability distribution is derived from the statistics of the network deep features and is almost irrelevant to specific image content (see Sec. 6.3). In summary, SRGA satisfies all four properties for GA design in Sec. 2. SRGA is correlated with both the model itself and the test data. It is a relative indicator that measures the difference of processing effects. It is not sensitive to specific image content but the degradation. Also, SRGA is a statistical approach without relying on learning process.

Datasets	Has GT?	Syn/Real?	Description
PIES-Clean	✓	Syn	Image patches collected from DIV2K-valid100, BSDS100, Urban100 and General100 datasets. The corresponding LR patches are downsampled using matlab <code>bicubic</code> function.
PIES-Blur	✓	Syn	Additionally apply Gaussian blur on PIES800-Clean dataset. The blur kernel width is sampled in {0.5, 1.0, 1.5, 2.0, 2.5, 3.0, 3.5, 4.0, 4.5, 5.0, 5.5, 6.0, 6.5, 7.0, 7.5, 8.0} (16 subsets in total).
PIES-AnisoBlur	✓	Syn	Additionally apply anisotropic Gaussian blur on PIES800-Clean dataset. The kernel size is 21, the kernel width is uniformly sampled in [0,6,5] and the rotation is uniformly sampled in [0, π].
PIES-Noise	✓	Syn	Add Gaussian noise on PIES800-Clean dataset. The noise level is sampled in {5, 10, 15, 20, 25, 30, 35, 40, 45, 50} (10 subsets in total).
PIES-BlurNoise	✓	Syn	Apply both Gaussian blur and Gaussian noise. The blur kernel width is sampled in {1, 2, 4, 6} and the noise level is sampled in {10, 20, 30} (12 subsets in total).
PIES-RealCam	✓	Real	Image patches selected from RealSR dataset [4]. RealSR dataset consists of LR-HR image pairs obtained by adjusting the lens of two digital single lens reflex (DSLR) cameras (Nikon D810 and Cannon 5D3).
PIES-RealLQ	✗	Real	Image patches collected from the Internet, containing real-world images of various distortion types and degrees.

Table 2. The Description of Patch-based Image Evaluation Dataset (PIES). It includes both synthetic and real-world images with fine-grained degradation types.

5 Patch-based Image Evaluation Set

For SR task, classical test datasets include Set5 [2], Set14 [45], BSD100 [18], Urban100 [7] and DIV2K-valid100 [33]. Most methods evaluate their performance on these public datasets. However, these datasets do not provide sufficient fine-grained and continuous degradation types, making it difficult to precisely evaluate the generalization performance. Moreover, test images with large resolution require tremendous computational cost and storage to estimate the feature distributions. Therefore, we propose a new fine-grained Patch-based Image Evaluation Set (PIES). It contains a variety of test images with different degradation types and degrees, including both **synthetic** and **real-world** degradations. PIES dataset has the following characteristics: i) Patch-based. Instead of evaluating a whole image with large resolution, we focus on image patches with relatively small resolution (128×128 for HR and 32×32 for LR, *i.e.* $\times 4$ SR). The degradation type and degree in one patch can be considered homogeneous and spatially invariant, which can facilitate analysis. ii) Fine-grained degradation types. PIES dataset contains different types of common degradation and covers a wide range of degradation degrees. The descriptions for PIES are summarized in Tab. 2. Each subset contains 800 patches. With PIES dataset, we can both evaluate the model performance and generalization ability on a unified platform.

Notably, researchers can also define their own test dataset and reference dataset according to the practical needs. The proposed SRGA index is not dependent on specific datasets and does not require paired GT images.

6 Benchmarking Deep SR Models

In this paper, we select representative SR methods to benchmark their generalization ability with PIES dataset, including SRResNet [11], IKC [6], DAN [15], DASR [35], Real-ESRGAN [37], BSRGAN [47] and SwinIR [12]. We train SRResNet with different training data as baselines. For other methods, we directly adopt their released pre-trained models. IKC, DAN and DASR methods mainly focus on blur degradation, thus their released model cannot deal with noisy images. Real-ESRGAN, BSRGAN and SwinIR-GAN are trained with multiple synthetic complex degraded data. We conduct experiments on $\times 4$ SR. Since the

blind SR methods are supposed to perform well on clean input images, we select PIES-Clean dataset as the reference dataset, and then calculate the SRGA index between the reference and other test datasets. A smaller SRGA value suggests that the model can well generalize to the test dataset.³

In this section, we first conduct validation experiments to verify the correctness of the proposed SRGA index, and benchmark the generalization ability of existing models. Then, we compare SRGA with IQA as generalization ability measurements. Due to the space limit, the complete quantitative and qualitative results are included in the supplementary file.

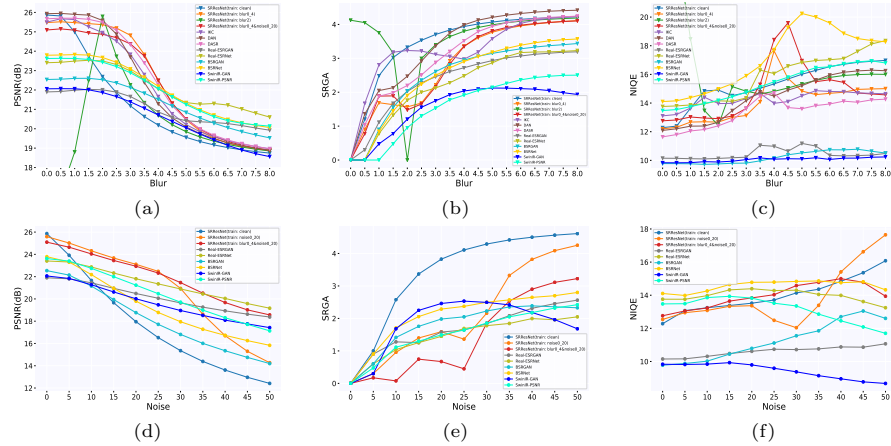


Fig. 4. The PSNR curves (a)&(d), SRGA curves (b)&(e) and NIQE curves (c)&(f) of different models on blur and noise degradations, respectively. SRGA successfully quantifies the model generalization ability. Further, it can reflect more precise information about the model generalization ability. The detailed quantitative values are listed in the supplementary file.

6.1 Sanity Check for SRGA

As there is no ground truth or human label for generalization ability, it is hard to evaluate the effectiveness of GA index directly. Nevertheless, we can construct some cases for sanity check. *Case 1*: The baseline model SRResNet trained only with clean LR data is supposed to have poor generalization ability to handle blur images. The PSNR value of this model reaches the highest on the clean input data, and then decreases rapidly as the blur degree increases (Fig. 4(a)). After involving blur LR data into training, SRResNet (train: blur0-4) is eligible to restore blur images: the PSNR value decreases slowly especially in the range of blur level [0, 3]. In Fig. 4(b), we observe that the SRGA curves have the same trend with the PSNR curves in such cases. For example, the SRGA

³ Note that model like SRResNet (train: blur2) performs well on blur2 images, thus, the reference dataset should be selected as PIES-Blur2 instead of PIES-Clean.

curve of SRResNet (train: clean) is steadily increasing, while the SRGA curve of SRResNet (train: blur0-4) grows slower and its values are all lower than that of SRResNet (train: clean). Especially in blur range [0, 3], the SRGA values of SRResNet (train: blur0-4) only change a little within a small range. The SRGA curves successfully depict the model generalization ability in a quantitative manner. Similar results are also observed in baseline model SRResNet (train: clean) and SRResNet (train: noise0-20) (see Fig. 4(d)&(e)). *Case 2*: In another extreme case, we train a SRResNet model with only blur2 data. The SRGA curve can also successfully reflect the trend of generalization. *Case 3*: SRResNet (train: clean) and SRResNet (train: noise0-20) have similar poor generalization trend on blur degradation; but SRResNet (train: noise0-20) has better generalization than SRResNet (train: clean) on noise degradation (see Tab. 3). The SRGA results are consistent with our common sense. In principal, SRGA is theoretically and experimentally sound. It provides us with a tool to quantitatively measure the generalization, which is more reliable than intuitive judgment.

Methods	PIES-Blur	PIES-AnisoBlur	PIES-Noise	PIES-BlurNoise	PIES-RealCam	PIES-RealLQ
SRResNet (train: clean)	3.639 ₍₁₃₎	3.615 ₍₁₃₎	3.727 ₍₉₎	3.454 ₍₁₀₎	3.563 ₍₁₁₎	3.825 ₍₈₎
SRResNet (train: blur0-4)	2.967 ₍₇₎	2.880 ₍₈₎	-	3.366 ₍₉₎	3.125 ₍₆₎	3.811 ₍₆₎
SRResNet (train: noise0-20)	3.623 ₍₁₂₎	3.605 ₍₁₂₎	2.325 ₍₈₎	3.167 ₍₈₎	3.547 ₍₁₀₎	3.827 ₍₉₎
SRResNet (train: blur0-4&noise0-20)	2.978 ₍₈₎	2.820 ₍₇₎	1.574 ₍₂₎	2.901 ₍₆₎	2.566 ₍₁₎	3.736 ₍₃₎
IKC	3.416 ₍₁₀₎	3.375 ₍₁₁₎	-	-	3.432 ₍₉₎	3.845 ₍₁₀₎
DAN	3.534 ₍₁₁₎	3.310 ₍₁₀₎	-	-	3.937 ₍₁₃₎	4.070 ₍₁₂₎
DASR	3.248 ₍₉₎	3.157 ₍₉₎	-	-	3.770 ₍₁₂₎	4.033 ₍₁₁₎
Real-ESRGAN	2.480 ₍₄₎	2.500 ₍₆₎	1.791 ₍₄₎	2.692 ₍₃₎	3.301 ₍₇₎	3.823 ₍₇₎
Real-ESRNet	2.336 ₍₃₎	2.456 ₍₅₎	1.566 ₍₁₎	2.900 ₍₅₎	2.787 ₍₃₎	3.770 ₍₄₎
BSRGAN	2.592 ₍₅₎	2.397 ₍₄₎	1.946 ₍₅₎	2.850 ₍₄₎	2.872 ₍₅₎	3.796 ₍₅₎
BSRNet	2.598 ₍₆₎	2.339 ₍₃₎	2.254 ₍₇₎	2.964 ₍₇₎	2.686 ₍₂₎	4.345 ₍₁₃₎
SwinIR-GAN	1.639 ₍₁₎	1.852 ₍₂₎	1.996 ₍₆₎	2.435 ₍₂₎	3.379 ₍₈₎	3.662 ₍₂₎
SwinIR-PSNR	1.668 ₍₂₎	1.727 ₍₁₎	1.685 ₍₃₎	2.297 ₍₁₎	2.826 ₍₄₎	3.655 ₍₁₎

Table 3. Average results (mSRGA) of generalization ability of representative SR networks. The null value indicates that the method cannot handle this type of degradation. The reference dataset is excluded when calculating the average. PIES-Blur, PIES-Noise and PIES-BlurNoise each contain multiple subdatasets. Since models may perform inconsistently on different degrees of degraded data, the average value may not reflect the actual situation. We recommend to refer to the detailed results in the supplementary file. (0 ~ 2: well generalized; 2 ~ 3: mediocre; > 3: poor)

6.2 Evaluating the Model Generalization Ability

Model generalization ability measures the difference of processing effects on different types of input data. Note that the generalization ability is not equal to the output image quality. The benchmarking results are summarized in Tab. 3. Complete results and analysis of real datasets are in the supplementary file.

Blur degradation. Fig. 4(b) summarizes the distances of the resulting feature distributions between clean LR input dataset and degraded input datasets with various blur levels. Smaller value means the model can well generalize to the test dataset. Larger SRGA values imply the model processes the input degradation more differently than the chosen reference dataset. As can be seen, the distances of SRResNet (train: blur0-4) are continuously smaller than SRResNet

(train: clean), which is intuitive and reasonable. The results can successfully describe the model performance change in a quantitative and analytical manner. For mild blur degradation (blur [0, 3]), DAN surpasses previous method IKC. However, when the blur degradation increases, the generalization ability of DAN becomes worse, indicating that DAN can only well generalized within mild degradation region. Among all the methods, SwinIR yields excellent generalization performance. Models trained with more degradations are likely to have better generalization despite that the absolute performance could deteriorate.

Noise degradation. As show in Fig. 4(e), with the input noise level increases, the feature distributions become more divergent from that of the input clean data. When the noise level exceeds the range that the model can handle (denoise), the SRGA curves of SRResNet increase dramatically. It is noteworthy that SwinIR-GAN shows peculiar characteristics when the noise level is larger. The distance of the feature distributions between the clean input and severe noise input becomes smaller. The visual results of SwinIR-GAN can give a reasonable explanation and can well embody the superiority of the proposed distribution-based GA metric (see Fig. 5). The outputs of SwinIR-GAN on large noises look more realistic, while the results of other methods contain obvious noise residues or artifacts. SwinIR-GAN tends to regenerate imaginary textures based on the noises. Although the generated images are different from the GT images in content, the output images look realistic without obvious artifacts. However, if we use the IQAs (especially reference-based IQA) to deduce the model generalization ability, such important phenomenon and observation cannot be perceived (see navy blur curves in Fig. 4(d)&(e)). More discussions are in Sec. 6.3.



Fig. 5. Visual results on PIES-Noise dataset. Note that PSNR and NIQE evaluate the **individual image quality**, while SRGA measures the model generalization (the consistency of processing effect) across different **degraded datasets**.

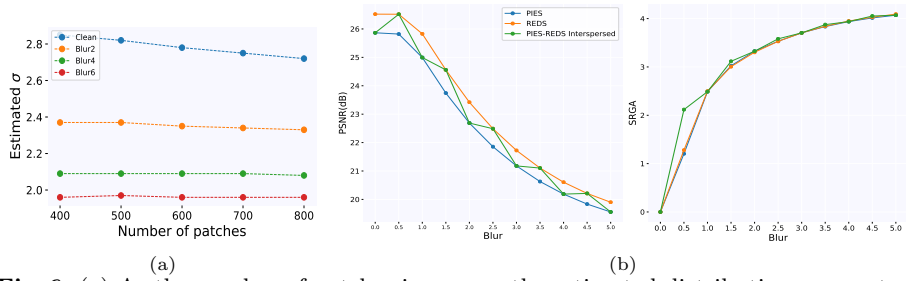


Fig. 6. (a) As the number of patches increases, the estimated distribution parameters gradually converge. (b) If the image contents are not aligned across degradations, PSNR values will fluctuate since it is heavily sensitive to the image contents while SRGA curves are more stable. “PIES-REDS Interspersed” means that the data in each blur level are interspersed by PIES and REDS.

6.3 Comparing SRGA with IQA

Notably, GA and IQA are conceptually different. *They are two different but complementary facets of evaluating the model. We are not proposing GA to supplant IQA.* Previously, however, since there is not any viable metric for evaluating the model generalization, people tend to utilize IQA to measure the performance and to deduce the generalization. Notwithstanding, there are several limitations of IQA for measuring model generalization ability. In the following, we illustrate the advantages of SRGA and limitations of IQA in five aspects.

SRGA vs. PSNR in sensitivity of image content. The proposed SRGA metric stems from the statistical characteristics of deep features of SR model: for a given model, different input degradation types will lead to different feature probability distributions, and such distributions are less sensitive to the image content but have higher response to image degradation, as illustrated in Sec. 4.3. Similar property is also observed in previous literatures [19,20,14,39]. We further validate this property. We select different numbers of image patches from PIES-Blur dataset to fit the corresponding distribution parameters (σ and α) using SRResNet(train:clean) model. Thus, the contents of the selected image sets with different numbers of patches are inconsistent. The patches are randomly selected and each setting is repeated three times. As shown in Fig. 6(a), with the increase of patch number, the estimated parameters gradually converge. Moreover, we select different datasets at different blur levels, so that the contents of the images are not aligned. For example, the data for clean, blur1, and blur2 are from the PIES dataset, and the data for blur0.5, blur1.5, and blur2.5 are from the REDS [23] dataset. Fig. 6(b) plots the corresponding PSNR and SRGA curves. The PSNR values are largely affected by the image content, leading to a fluctuating PSNR curve (not monotonic). But the SRGA curve can still depict the generalization trend of the model, despite of the fact that we use different datasets for calculation.⁴

⁴ In this experiment, PIES-Clean is selected as the reference dataset.

SRGA vs. PSNR in luminance jitter. Another advantageous property of SRGA is that it is more robust to image luminance jitter, which is a common photographic disturbance in real camera imaging. To validate the robustness of SRGA, we manually shift the luminance of the test PIES-Blur images and maintain the original luminance of the reference PIES-Clean dataset. As revealed in Fig. 7, when the global luminance jitter is within $[-10, +20]$, SRGA is basically unaffected and maintains good stability. However, PSNR is sensitive to such disturbance, since it measures the absolute distance between paired pixels. This shows the great superiority of SRGA over IQA. SRGA can deal with such disturbance since the PCA operation has subtracted the mean of the features beforehand. If the brightness changes too much, SRGA will also change, because the input distribution has altered a lot. This is equivalent to adding a new degradation to the input image, which is out of the scope of this discussion.

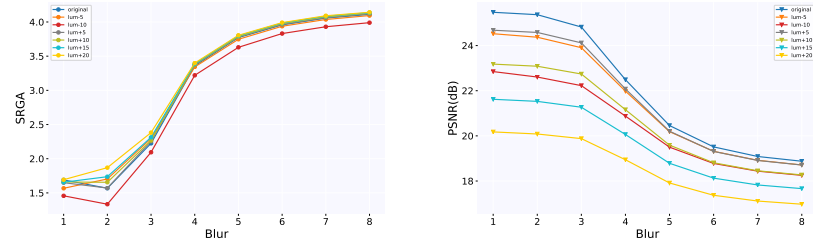


Fig. 7. When the global brightness between the test and reference images is not aligned (luminance jitter), SR models may still produce good SR results, but IQA will be severely affected and the PSNR values will be completely different. Nevertheless, SRGA is more robust to such disturbance.

SRGA vs. NR-IQA in performance stability. For no-reference IQA, like NIQE, it is widely acknowledged that it is unstable and less accurate [5,47]. As shown in Fig. 4(c)&(f), NIQE values fluctuate greatly, compared with PSNR. In Fig. 5, the results of SwinIR-GAN on Noise > 20 look visually similar, but their NIQE values differ a lot. This can be attributed to the fact that NIQE is simply determined by limited handcrafted features. Besides NIQE, Gu *et al.* [8,5] also demonstrate that other existing NR-IQAs are far from satisfactory. Inaccuracy and instability make NR-IQA unsuitable as a good GA.

SRGA vs. IQA in real data without GT. Full-reference IQA, like PSNR and SSIM, requires paired ground-truth (GT) images, which is impractical in real scenarios. No-reference IQA is inaccurate and instable as mentioned before. However, SRGA does not rely on paired reference images, since it considers the distance between statistical feature distributions. As shown in Tab. 3, SRGA can be successfully applied on real-world datasets.

Failure cases of IQA. IQA cannot precisely reflect the model generalization. For example, when the noise level is extremely severe (*e.g.*, larger than 30), most methods are unable to produce visually pleasing images. However, SwinIR-GAN can produce relatively realistic output images by generating imag-

inary textures (see Fig. 5). This demonstrates SwinIR’s powerful learning and generation capabilities. The PSNR curve of SwinIR continues to decline, while the SRGA curve well depicts the trend of model generalization (see navy blur curves in Fig. 4(d)&(e)). This suggests the intrinsic superiority of SRGA.

These aforementioned issues have prevented IQA from being a qualified GA. In fact, IQA and SRGA are complementary. IQA can be used to evaluate the absolute model performance and help select the reference dataset for SRGA. If a model has extremely low IQA score, such as a randomly initialized network, it is meaningless to discuss its generalization ability, and there is no need to consider its SRGA value. Hence, IQA and SRGA should cooperate with each other.

7 Limitations

Since we are the first to propose a generalization assessment metric for SR networks, our work has several limitations. First, SRGA requires a relatively large amount of computation and storage. Second, unlike IQA, it is hard to subjectively evaluate GA by user study, as GA requires to measure the processing consistency between degraded datasets, not individual images. Third, SRGA is a statistical method, which cannot be directly used as a loss function to optimize the network. But we can mimic its behavior to guide the design of future models.

References

1. Bell-Kligler, S., Shocher, A., Irani, M.: Blind super-resolution kernel estimation using an internal-gan. arXiv preprint arXiv:1909.06581 (2019) [1](#)
2. Bevilacqua, M., Roumy, A., Guillemot, C., Alberi-Morel, M.L.: Low-complexity single-image super-resolution based on nonnegative neighbor embedding (2012) [9](#)
3. Blau, Y., Mechrez, R., Timofte, R., Michaeli, T., Zelnik-Manor, L.: The 2018 pirm challenge on perceptual image super-resolution. In: Proceedings of the European Conference on Computer Vision (ECCV) Workshops. pp. 0–0 (2018) [2](#)
4. Cai, J., Zeng, H., Yong, H., Cao, Z., Zhang, L.: Toward real-world single image super-resolution: A new benchmark and a new model. In: Proceedings of the IEEE/CVF International Conference on Computer Vision. pp. 3086–3095 (2019) [9](#)
5. Gu, J., Cai, H., Dong, C., Ren, J.S., Qiao, Y., Gu, S., Timofte, R.: Ntire 2021 challenge on perceptual image quality assessment. In: Proceedings of the IEEE/CVF Conference on Computer Vision and Pattern Recognition. pp. 677–690 (2021) [2](#), [14](#)
6. Gu, J., Lu, H., Zuo, W., Dong, C.: Blind super-resolution with iterative kernel correction. In: Proceedings of the IEEE/CVF Conference on Computer Vision and Pattern Recognition. pp. 1604–1613 (2019) [1](#), [9](#), [19](#), [20](#)
7. Huang, J.B., Singh, A., Ahuja, N.: Single image super-resolution from transformed self-exemplars. In: Proceedings of the IEEE conference on computer vision and pattern recognition. pp. 5197–5206 (2015) [9](#)
8. Jinjin, G., Haoming, C., Haoyu, C., Xiaoxing, Y., Ren, J.S., Chao, D.: Pipal: a large-scale image quality assessment dataset for perceptual image restoration. In: European Conference on Computer Vision. pp. 633–651. Springer (2020) [2](#), [14](#)

9. Keskar, N.S., Mudigere, D., Nocedal, J., Smelyanskiy, M., Tang, P.T.P.: On large-batch training for deep learning: Generalization gap and sharp minima. arXiv preprint arXiv:1609.04836 (2016) [2](#)
10. Kong, X., Liu, X., Gu, J., Qiao, Y., Dong, C.: Reflash dropout in image super-resolution. arXiv preprint arXiv:2112.12089 (2021) [2](#)
11. Ledig, C., Theis, L., Huszár, F., Caballero, J., Cunningham, A., Acosta, A., Aitken, A., Tejani, A., Totz, J., Wang, Z., et al.: Photo-realistic single image super-resolution using a generative adversarial network. In: Proceedings of the IEEE conference on computer vision and pattern recognition. pp. 4681–4690 (2017) [9](#)
12. Liang, J., Cao, J., Sun, G., Zhang, K., Van Gool, L., Timofte, R.: Swinir: Image restoration using swin transformer. In: Proceedings of the IEEE/CVF International Conference on Computer Vision. pp. 1833–1844 (2021) [3, 9, 20, 21](#)
13. Liu, A., Liu, Y., Gu, J., Qiao, Y., Dong, C.: Blind image super-resolution: A survey and beyond. arXiv preprint arXiv:2107.03055 (2021) [1](#)
14. Liu, Y., Liu, A., Gu, J., Zhang, Z., Wu, W., Qiao, Y., Dong, C.: Discovering “semantics” in super-resolution networks. arXiv preprint arXiv:2108.00406 (2021) [5, 13](#)
15. Luo, Z., Huang, Y., Li, S., Wang, L., Tan, T.: Unfolding the alternating optimization for blind super resolution. arXiv preprint arXiv:2010.02631 (2020) [1, 9, 19, 20](#)
16. Maeda, S.: Unpaired image super-resolution using pseudo-supervision. In: Proceedings of the IEEE/CVF Conference on Computer Vision and Pattern Recognition. pp. 291–300 (2020) [1](#)
17. Mallat, S.G.: A theory for multiresolution signal decomposition: the wavelet representation. In: Fundamental Papers in Wavelet Theory, pp. 494–513. Princeton University Press (2009) [5](#)
18. Martin, D., Fowlkes, C., Tal, D., Malik, J.: A database of human segmented natural images and its application to evaluating segmentation algorithms and measuring ecological statistics. In: Proceedings Eighth IEEE International Conference on Computer Vision. ICCV 2001. vol. 2, pp. 416–423. IEEE (2001) [9](#)
19. Mittal, A., Moorthy, A.K., Bovik, A.C.: No-reference image quality assessment in the spatial domain. IEEE Transactions on image processing **21**(12), 4695–4708 (2012) [5, 13](#)
20. Mittal, A., Soundararajan, R., Bovik, A.C.: Making a “completely blind” image quality analyzer. IEEE Signal processing letters **20**(3), 209–212 (2012) [2, 5, 13](#)
21. Moorthy, A.K., Bovik, A.C.: Statistics of natural image distortions. In: 2010 IEEE International Conference on Acoustics, Speech and Signal Processing. pp. 962–965. IEEE (2010) [5](#)
22. Moulin, P., Liu, J.: Analysis of multiresolution image denoising schemes using generalized gaussian and complexity priors. IEEE transactions on Information Theory **45**(3), 909–919 (1999) [5](#)
23. Nah, S., Baik, S., Hong, S., Moon, G., Son, S., Timofte, R., Mu Lee, K.: Ntire 2019 challenge on video deblurring and super-resolution: Dataset and study. In: Proceedings of the IEEE/CVF Conference on Computer Vision and Pattern Recognition Workshops. pp. 0–0 (2019) [13](#)
24. Neyshabur, B., Bhojanapalli, S., McAllester, D., Srebro, N.: Exploring generalization in deep learning. arXiv preprint arXiv:1706.08947 (2017) [3, 18](#)
25. Neyshabur, B., Bhojanapalli, S., Mcallester, D., Srebro, N.: Exploring generalization in deep learning. In: Guyon, I., Luxburg, U.V., Bengio, S., Wallach, H., Fergus, R., Vishwanathan, S., Garnett, R. (eds.)

Advances in Neural Information Processing Systems. vol. 30. Curran Associates, Inc. (2017), <https://proceedings.neurips.cc/paper/2017/file/10ce03a1ed01077e3e289f3e53c72813-Paper.pdf> 2

26. Neyshabur, B., Tomioka, R., Srebro, N.: In search of the real inductive bias: On the role of implicit regularization in deep learning. In: ICLR (Workshop) (2015), <http://arxiv.org/abs/1412.6614> 2
27. Novak, R., Bahri, Y., Abolafia, D.A., Pennington, J., Sohl-Dickstein, J.: Sensitivity and generalization in neural networks: an empirical study (2018) 2
28. Ruderman, D.L.: The statistics of natural images. Network: computation in neural systems 5(4), 517 (1994) 5
29. Ruderman, D.L., Bialek, W.: Statistics of natural images: Scaling in the woods. Physical review letters 73(6), 814 (1994) 5
30. Sharifi, K., Leon-Garcia, A.: Estimation of shape parameter for generalized gaussian distributions in subband decompositions of video. IEEE Transactions on Circuits and Systems for Video Technology 5(1), 52–56 (1995) 7
31. Shocher, A., Cohen, N., Irani, M.: “zero-shot” super-resolution using deep internal learning. In: Proceedings of the IEEE conference on computer vision and pattern recognition. pp. 3118–3126 (2018) 1
32. Srivastava, N., Hinton, G., Krizhevsky, A., Sutskever, I., Salakhutdinov, R.: Dropout: a simple way to prevent neural networks from overfitting. The journal of machine learning research 15(1), 1929–1958 (2014) 2
33. Timofte, R., Agustsson, E., Van Gool, L., Yang, M.H., Zhang, L.: Ntire 2017 challenge on single image super-resolution: Methods and results. In: Proceedings of the IEEE conference on computer vision and pattern recognition workshops. pp. 114–125 (2017) 9
34. Wainwright, M.J., Simoncelli, E.P.: Scale mixtures of gaussians and the statistics of natural images. In: Nips. vol. 12, pp. 855–861. Citeseer (1999) 5
35. Wang, L., Wang, Y., Dong, X., Xu, Q., Yang, J., An, W., Guo, Y.: Unsupervised degradation representation learning for blind super-resolution. In: Proceedings of the IEEE/CVF Conference on Computer Vision and Pattern Recognition. pp. 10581–10590 (2021) 1, 9, 19, 20
36. Wang, X., Li, Y., Zhang, H., Shan, Y.: Towards real-world blind face restoration with generative facial prior. In: Proceedings of the IEEE/CVF Conference on Computer Vision and Pattern Recognition. pp. 9168–9178 (2021) 2
37. Wang, X., Xie, L., Dong, C., Shan, Y.: Real-esrgan: Training real-world blind super-resolution with pure synthetic data. In: Proceedings of the IEEE/CVF International Conference on Computer Vision. pp. 1905–1914 (2021) 1, 2, 9, 19, 20, 21
38. Wang, X., Yu, K., Wu, S., Gu, J., Liu, Y., Dong, C., Qiao, Y., Change Loy, C.: Esrgan: Enhanced super-resolution generative adversarial networks. In: Proceedings of the European conference on computer vision (ECCV) workshops. pp. 0–0 (2018) 19
39. Wang, Y., Cao, Y., Zha, Z.J., Zhang, J., Xiong, Z.: Deep degradation prior for low-quality image classification. In: Proceedings of the IEEE/CVF Conference on Computer Vision and Pattern Recognition. pp. 11049–11058 (2020) 13
40. Wang, Z., Bovik, A.C., Sheikh, H.R., Simoncelli, E.P.: Image quality assessment: from error visibility to structural similarity. IEEE transactions on image processing 13(4), 600–612 (2004) 4
41. Wold, S., Esbensen, K., Geladi, P.: Principal component analysis. Chemometrics and intelligent laboratory systems 2(1-3), 37–52 (1987) 6

42. Xiong, Y., Jing, Y., Chen, T.: Abnormality detection based on the kullback–leibler divergence for generalized gaussian data. *Control Engineering Practice* **85**, 257–270 (2019) [8](#)
43. Yang, T., Ren, P., Xie, X., Zhang, L.: Gan prior embedded network for blind face restoration in the wild. In: *Proceedings of the IEEE/CVF Conference on Computer Vision and Pattern Recognition*. pp. 672–681 (2021) [2](#)
44. Yuan, Y., Liu, S., Zhang, J., Zhang, Y., Dong, C., Lin, L.: Unsupervised image super-resolution using cycle-in-cycle generative adversarial networks. In: *Proceedings of the IEEE Conference on Computer Vision and Pattern Recognition Workshops*. pp. 701–710 (2018) [1](#)
45. Zeyde, R., Elad, M., Protter, M.: On single image scale-up using sparse-representations. In: *International conference on curves and surfaces*. pp. 711–730. Springer (2010) [9](#)
46. Zhang, C., Bengio, S., Hardt, M., Recht, B., Vinyals, O.: Understanding deep learning (still) requires rethinking generalization. *Communications of the ACM* **64**(3), 107–115 (2021) [2](#)
47. Zhang, K., Liang, J., Van Gool, L., Timofte, R.: Designing a practical degradation model for deep blind image super-resolution. *arXiv preprint arXiv:2103.14006* (2021) [1](#), [9](#), [14](#), [19](#), [20](#), [21](#)
48. Zhang, R., Isola, P., Efros, A.A., Shechtman, E., Wang, O.: The unreasonable effectiveness of deep features as a perceptual metric. In: *Proceedings of the IEEE conference on computer vision and pattern recognition*. pp. 586–595 (2018) [4](#)
49. Zhou, P., Feng, J.: Understanding generalization and optimization performance of deep cnns. In: *International Conference on Machine Learning*. pp. 5960–5969. PMLR (2018) [3](#), [18](#)

A Appendix

A.1 Generalization in Super-Resolution Task

As a commonly-used definition, generalization is the ability of your model, after being trained to digest new data and make accurate predictions [24,49]. There are three key components – model, data and prediction, which all have specific meanings in SR task. (1) Model in this paper refers to the SR network. Generalization should be a property of the network, NOT output images. (2) Data refers to the input images with specific degradations. Generalization should be evaluated on degradations, NOT individual images. (3) Prediction refers to the processing effect of the output image. Generalization should measure the consistency of the processing effects across different input degradations, NOT absolute quality evaluation values. For example, an appropriate description would be: if SR-net trained with data-A (well-performing domain) can achieve similar performance on data-B, SR-net generalizes well on data-B.

A.2 Blind and Real-world Super-Resolution

Blind or real-world super-resolution aims at recovering and super-resolving an input low-resolution (LR) image with unknown and real-world degradation to a

high-resolution (HR) version. Formally, a classical image degradation model is formulated as follows:

$$I^{LR} = (I^{HR} \otimes k) \downarrow_s + n, \quad (10)$$

where I^{HR} is the HR image, I^{LR} is the degraded LR image, \otimes denotes the convolution operation. There are mainly three types of degradation in this model, *i.e.*, blur kernel k , additive noise n and the downsampling operation \downarrow_s . For blind SR setting, the degradation information is unavailable during the training process. Generally, most current methods follow this degradation model or its variants [6,15,37]. Recently, BSRGAN [47] proposes a practical image degradation that consists of randomly shuffled blur, downsampling and noise degradations. Real-ESRGAN [37] further introduces a high-order degradation modeling process, *i.e.*, the degradations are modeled with several repeated degradation processes, each process being the classical degradation model.

A.3 Implementation Details

As mentioned in the main paper, for all the SR models, we extract the output features of the second last layer to calculate the SRGA index. An simplified illustration is depicted in Fig. 8. The deepest layer contains all the processed information to produce the final results. There is no more processing layer afterwards. Thus, it is reasonable to use this layer to compute SRGA. Another reason is that different models have different architectures, it is convenient and universal to adopt the last layer.

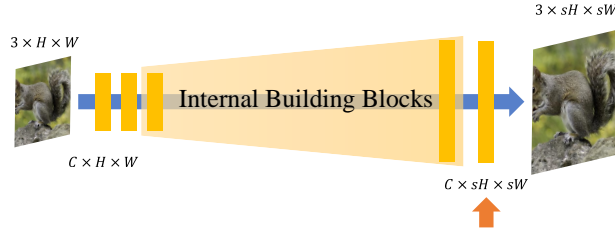


Fig. 8. Simplified architecture for arbitrary SR networks. We extract the deepest features (pointed by the arrow) to calculate the SRGA index.

For SRResNet, we follow the network design and training settings depicted in [38]. We train SRResNet with different training data as baseline, to suggest the effectiveness of SRGA. For IKC [6], DAN [15] and DASR [35], we directly use their released trained models to inference. As these methods mainly focus on restoring and super-resolving blurry images, we do not apply them on noisy inputs. We use the isotropic blur version of DASR. For Real-ESRGAN [37] and

BSRGAN [47], they are proposed for blind and real settings. They adopt multiple and complex degradation models to generate sufficient training data, which covers a wide range of diverse distorted images. SwinIR [12] is a newly proposed transformer-based image restoration framework. We adopt the released model with the same training setting as BSRGAN, which aims to tackle blind SR.

A.4 Complete Benchmarking Results

We present the completee quantitative results in this section. The benchmarking results of model generalization ability based on SRGA are summarized in Tab. 4, 5, 6, 7 and 8 . The corresponding SRGA curves are already shown in the main paper. In addition, we also show the PSNR, SSIM, LPIPS, NIQE values, which evaluate the output image quality and measure the model performance, as shown in Tab. 9, 10, 11, 12, 13, 14, 15, 16, 17, 18, 19, 20 and 21. The corresponding curves are depicted in Fig. 9 and 10.

It can be observed that if we train SRResNet with degraded inputs, the model generalization will be boosted. This is reasonable and confirms that the model generalization ability is related to the model itself and the training data. **For blur degradation**, interestingly, DAN [6] has better model performance and generalization ability on mild degraded data (blur [0, 2.5]) than SRResNet (train: blur0-2) and IKC. However, when the blur level is larger, its performance (PSNR, SSIM) and generalization (SRGA) deteriorate dramatically. The proposed SRGA metric successfully describes such phenomenon. Another important observation is that methods like Real-ESRGAN [37], BSRGAN [47] and SwinIR [12] have relatively more stable and better generalization ability, especially for severe degraded data. Particularly, when the blur level is larger than 5, SRResNet, IKC [6], DAN [15] and DASR [35] all fail to reconstruct the sharp images, while Real-ESRGAN, BSRGAN and SwinIR-GAN can still generate realistic images with sharp textures (see Fig. 11 and 12). It shows the superiority of such newly-proposed methods. **For noise degradation**, the observation is even more interesting. When noise level is extremely severe (*e.g.*, noise level is larger than 30), most methods are unable to produce visually pleasing images. The results of SRResNet contains many noise residue and artifacts. The results of Real-ESRGAN (Real-ESRNet) are over-smoothed. The results of BSRGAN (BSRNet) are unsatisfactory with severe color distortion and artifacts. Nevertheless, SwinIR-GAN can produce relatively realistic output images by generating sharpened textures. Although the generated images are not consistent with the ground truth image, they look realistic with few noise residue and artifacts. SwinIR-GAN seems to treat the severe noisy input as a kind of texture and generate more textured details according to the noise distribution. This demonstrates SwinIR’s powerful learning and generation capabilities. If we use IQAs to measure the model generalization ability, it is hard to observe such phenomenon, while SRGA successfully helps us discover such interesting fact. Specifically, the PSNR values continuously decrease when the noise level become larger, since it measures the pixel-wise distance between the SR results and the GT images. However, SRGA can help us find that the processing effect

of SwinIR-GAN on severe noisy images is not continuously deteriorating. For severe noisy images, SwinIR-GAN can still produce visually plausible realistic results. **For anisotropic blur degradation**, SRGA can also compare the generalization ability of different models. Methods like BSRGAN, Real-ESRGAN and SwinIR still have good generalization.

Another advantage of the proposed SRGA is that it does not require any paired reference images as ground-truth (GT). Thus, it can be applied to evaluate the model generalization ability on **real-world** images. SwinIR [12], BSRGAN [47] and Real-ESRGAN [37] generalize well on PIES-RealCam dataset. SRResNet (train: blur0-4&noise0-20) has good generalization on this dataset as well. Note again, the generalization does not mean model performance. It just measures the difference in the processing effect of the model on different inputs. To fully evaluate the merits of a model, we need to assess it comprehensively, including model performance, generalization ability, number of parameters, computational cost, etc. SRGA only gives a new perspective for evaluating the model generalization ability, since there is no any quantitative metric for model generalization before.

A.5 Insights and Inspirations

With the proposed SRGA metric, we roughly evaluate the generalization ability of several representative SR models. Methods like Real-ESRGAN (Real-ESRNet), BSRGAN (BSRNet) and SwinIR, adopt abundant diverse complex degraded LR data into training, which covers a large number of degradation types and degrees. This has led to the fact that the PSNR and SSIM values of these models are not as good as other methods on the images with mild distortion, but as the image degradation becomes severer, this type of method gradually shows its advantages. Their performance is much more stable and less susceptible to input degradation changes. In other words, although their absolute performance is not the best, their generalization ability is much superior. This suggests that expanding the training datasets with more degraded data can indeed improve the model generalization ability. This observation confirms the superiority of this type of method for blind SR and real-world SR. It motivates us to develop more advanced SR methods with large capacity for multiple degradations.

Further, based on the mechanism of SRGA, if we can pose penalty or constraint to make the output feature distributions more unanimous, it is possible approach to improving the model generalization ability.

A.6 Statistical Characteristics of SR Deep Features

Tab. 22 shows the estimated GGD parameters for different models and different blur level inputs. If the model processes two different degradations with similar effects, their feature distributions will also be close. Based on the above properties, we build a statistical model to evaluate the model generalization ability.

In the main paper, we have conducted experiments to show the statistical characteristics of SR deep features: for a given model, different input degradation types will lead to different feature probability distributions, and such distributions are less sensitive to the image content but have higher response to image degradation.

A.7 Visualization of Output Images

The visual results of the output images produced by representative SR models are shown in Fig. 11, 12, 13, 14, 15, 16, and 17. From the visual results, we can see that Real-ESRGAN, BSRGAN, SwinIR-GAN achieve relatively better performance with visually pleasing output images.

A.8 Samples of PIES Dataset

Fig. 18, 19, and 20 show some samples of PIES dataset, including PIES-Blur, PIES-Noise, PIES-BlurNoise, PIES-RealCam and PIES-RealLQ. It is easy to create your own datasets to test the model generalization ability using SRGA. The proposed PIES dataset only provide a unified platform to evaluate the model. The proposed metric is not restricted to this dataset.

Methods	Clean	Blur Level															
		0.5	1.0	1.5	2.0	2.5	3.0	3.5	4.0	4.5	5.0	5.5	6.0	6.5	7.0	7.5	8.0
SRResNet (train: clean)	0.000	1.204	2.489	3.024	3.325	3.532	3.705	3.835	3.938	4.014	4.070	4.118	4.151	4.177	4.196	4.213	4.229
SRResNet (train: blur0.4)	0.000	0.903	1.690	1.633	1.568	1.681	2.225	2.930	3.358	3.607	3.772	3.880	3.958	4.011	4.057	4.089	4.111
SRResNet (train: blur2)	4.124	4.054	3.758	3.156	0.000	2.997	3.403	3.642	3.798	3.910	3.989	4.051	4.096	4.128	4.154	4.173	4.190
SRResNet (train: blur0.4+noise0.20)	0.000	0.778	1.886	1.892	1.477	1.653	2.164	2.831	3.349	3.641	3.809	3.911	3.978	4.026	4.057	4.086	4.105
IKC	0.000	1.672	2.810	3.181	3.231	3.216	3.116	3.056	2.975	3.184	3.582	3.854	4.031	4.125	4.177	4.211	4.231
DAN	0.000	1.362	2.049	2.134	2.471	2.919	3.367	3.750	3.987	4.126	4.210	4.274	4.323	4.362	4.390	4.407	4.419
DASR	0.000	1.041	1.881	1.987	2.199	2.511	2.878	3.202	3.520	3.791	3.944	4.048	4.120	4.167	4.208	4.226	4.245
Real-ESRGAN	0.000	0.301	1.114	1.672	2.025	2.279	2.458	2.612	2.722	2.836	2.934	3.015	3.068	3.120	3.151	3.180	3.192
Real-ESRNet	0.000	0.000	0.078	1.322	1.763	2.000	2.127	2.281	2.480	2.725	2.866	3.052	3.170	3.187	3.191	3.206	3.230
BSRGAN	0.000	0.000	0.903	1.556	2.041	2.356	2.610	2.814	2.947	3.061	3.147	3.217	3.280	3.333	3.373	3.403	3.437
BSRNet	0.000	0.000	0.845	1.447	1.903	2.241	2.496	2.719	2.905	3.056	3.181	3.294	3.387	3.459	3.516	3.549	3.570
SwinIR-GAN	0.000	0.000	0.477	0.778	1.204	1.556	1.748	1.929	2.037	2.090	2.124	2.121	2.107	2.090	2.049	1.987	1.934
SwinIR-PSNR	0.000	0.000	0.000	0.477	0.954	1.301	1.531	1.778	1.914	2.053	2.143	2.260	2.365	2.433	2.471	2.498	2.504

Table 4. Model generalization ability (SRGA) on PIES-Blur dataset. Small SRGA value denotes better generalization.

Methods	Clean	Noise Level									
		5	10	15	20	25	30	35	40	45	50
SRResNet (train: clean)	0.000	1.000	2.579	3.368	3.826	4.108	4.291	4.417	4.501	4.564	4.612
SRResNet (train: noise0_20)	0.000	0.301	0.954	1.398	1.591	1.362	2.161	3.323	3.818	4.087	4.253
SRResNet (train: blur0_4+noise0_20)	0.000	0.172	0.077	0.778	0.699	0.477	1.857	2.534	2.900	3.111	3.226
Real-ESRGAN	0.000	0.903	1.279	1.255	1.580	1.643	1.839	2.083	2.312	2.456	2.562
Real-ESRNet	0.000	0.602	1.041	1.255	1.447	1.690	1.778	1.845	1.996	1.959	2.049
BSRGAN	0.000	0.602	1.415	1.756	1.982	2.049	2.228	2.354	2.387	2.358	2.328
BSRNet	0.000	0.903	1.708	2.057	2.288	2.371	2.498	2.571	2.648	2.700	2.800
SwinIR-GAN	0.000	0.301	1.681	2.248	2.461	2.533	2.494	2.417	2.182	1.964	1.681
SwinIR-PSNR	0.000	0.477	1.114	1.301	1.491	1.643	1.857	2.049	2.179	2.320	2.423

Table 5. Model generalization ability (SRGA) on PIES-Noise dataset. Small SRGA value denotes better generalization.

Methods	Clean	Blur1			Blur2			Blur4			Blur6		
		10	20	30	10	20	30	10	20	30	10	20	30
SRResNet (train: clean)	0.000	1.771	3.744	4.282	1.934	3.665	4.260	3.037	3.535	4.239	3.266	3.476	4.224
SRResNet (train: blur0_4)	0.000	1.114	3.632	4.184	2.297	3.535	4.161	3.179	3.361	4.125	3.412	3.279	4.115
SRResNet (train: noise0_20)	0.000	2.459	2.539	1.079	3.253	3.261	2.630	3.833	3.827	3.427	4.037	4.030	3.630
SRResNet (train: blur0_4+noise0_20)	0.000	1.964	2.061	0.954	2.307	2.584	2.797	3.299	3.534	3.642	3.870	3.920	3.874
Real-ESRGAN	0.000	1.875	1.857	1.633	2.442	2.452	2.382	3.039	3.114	3.232	3.270	3.419	3.585
Real-ESRNet	0.000	1.663	2.025	2.253	2.332	2.624	2.868	3.093	3.383	3.575	3.448	3.687	3.852
BSRGAN	0.000	1.892	2.389	2.569	2.425	2.668	2.727	3.121	3.177	3.135	3.378	3.379	3.339
BSRNet	0.000	1.982	2.490	2.654	2.450	2.805	2.885	3.134	3.288	3.339	3.468	3.520	3.554
SwinIR-GAN	0.000	1.863	2.548	2.520	2.104	2.611	2.550	2.444	2.649	2.531	2.330	2.515	2.554
SwinIR-PSNR	0.000	1.322	1.806	2.004	1.839	2.086	2.301	2.358	2.604	2.814	2.550	2.825	3.053

Table 6. Model generalization ability (SRGA) on PIES-BlurNoise dataset. Small SRGA value denotes better generalization.

Methods	PIES-Clean			PIES-RealCam			PIES-RealLQ		
	PIES-Clean	PIES-RealCam	PIES-RealLQ	PIES-Clean	PIES-RealCam	PIES-RealLQ	PIES-Clean	PIES-RealCam	PIES-RealLQ
SRResNet (train: clean)	0.000			3.563			3.825		
SRResNet (train: blur0_4)	0.000			3.125			3.811		
SRResNet (train: noise0_20)	0.000			3.547			3.827		
SRResNet (train: blur0_4+noise0_20)	0.000			2.566			3.736		
IKC	0.000			3.432			3.845		
DAN	0.000			3.937			4.070		
DASR	0.000			3.770			4.033		
Real-ESRGAN	0.000			3.301			3.823		
Real-ESRNet	0.000			2.787			3.770		
BSRGAN	0.000			2.872			3.796		
BSRNet	0.000			2.686			4.345		
SwinIR-GAN	0.000			3.379			3.662		
SwinIR-PSNR	0.000			2.826			3.655		

Table 7. Model generalization ability (SRGA) on PIES-RealCam and PIES-RealLQ datasets. Small SRGA value denotes better generalization.

Methods	PSNR	SSIM	NIQE	SRGA
SRResNet (train: clean)	21.54	0.5692	15.14	3.615
SRResNet (train: blur0_4)	23.24	0.6564	15.27	2.880
SRResNet (train: noise0_20)	21.52	0.5665	15.18	3.605
SRResNet (train: blur0_4+noise0_20)	23.19	0.6513	15.48	2.820
IKC	23.16	0.6537	16.23	3.375
DAN	23.43	0.6636	15.80	3.310
DASR	23.49	0.6658	15.92	3.157
Real-ESRGAN	21.31	0.5771	10.84	2.500
Real-ESRNet	22.46	0.6247	15.32	2.456
BSRGAN	21.89	0.5831	9.93	2.397
BSRNet	22.98	0.6315	15.91	2.339
SwinIR-GAN	21.21	0.5762	10.36	1.852
SwinIR-PSNR	22.57	0.6347	15.16	1.727

Table 8. Model performance (PNSR, SSIM, NIQE) and model generalization ability (SRGA) on PIES-AnisoBlur dataset.

Methods	Clean	Blur Level															
		0.5	1.0	1.5	2.0	2.5	3.0	3.5	4.0	4.5	5.0	5.5	6.0	6.5	7.0	7.5	8.0
SRResNet (train: clean)	25.87	25.82	24.99	23.74	22.69	21.85	21.18	20.63	20.19	19.84	19.56	19.34	19.17	19.03	18.91	18.82	18.74
SRResNet (train: blur0.4)	25.48	25.52	25.47	25.43	25.37	25.19	24.82	23.83	22.49	21.31	20.46	19.89	19.51	19.26	19.09	18.97	18.88
SRResNet (train: blur2)	16.20	16.69	18.80	22.48	25.80	23.74	22.27	21.34	20.69	20.21	19.85	19.57	19.36	19.19	19.05	18.94	18.85
SRResNet (train: blur0.4+noise0.20)	25.10	25.15	25.08	24.95	24.87	24.70	24.38	23.75	22.50	21.32	20.51	19.97	19.61	19.34	19.15	19.00	18.89
IKC	25.50	25.67	25.63	25.26	24.96	24.52	23.84	22.80	21.66	20.77	20.21	19.84	19.59	19.38	19.21	19.08	18.97
DAN	25.94	25.95	25.90	25.86	25.59	24.88	23.70	22.39	21.28	20.56	20.09	19.75	19.48	19.27	19.12	18.99	18.90
DASR	25.67	25.70	25.70	25.65	25.45	25.08	24.35	23.40	22.27	21.19	20.47	19.99	19.66	19.41	19.23	19.09	18.97
Real-ESRGAN	21.90	21.92	21.99	22.03	22.01	21.89	21.66	21.30	20.87	20.58	20.41	20.36	20.32	20.27	20.20	20.16	19.93
Real-ESRNet	23.41	23.43	23.49	23.53	23.50	23.31	22.98	22.53	22.05	21.65	21.35	21.27	21.30	21.22	21.02	20.80	20.60
BSRGAN	22.54	22.56	22.60	22.60	22.53	22.36	22.13	21.83	21.51	21.17	20.84	20.55	20.29	20.05	19.85	19.68	19.53
BSRNet	23.79	23.80	23.83	23.80	23.67	23.43	23.26	22.66	21.19	21.72	21.31	20.97	20.70	20.48	20.30	20.17	20.06
SwinIR-GAN	22.06	22.07	22.06	22.01	21.87	21.66	21.39	21.06	20.71	20.38	20.05	19.73	19.42	19.14	18.90	18.71	18.56
SwinIR-PSNR	23.62	23.63	23.63	23.57	23.43	23.21	22.89	22.50	22.07	21.64	21.25	20.91	20.62	20.41	20.28	20.20	20.13

Table 9. Model performance (PSNR) on PIES-Blur dataset. Higher PSNR value denotes that the output images are closer to the ground truth images in content.

Methods	Clean	Blur Level															
		0.5	1.0	1.5	2.0	2.5	3.0	3.5	4.0	4.5	5.0	5.5	6.0	6.5	7.0	7.5	8.0
SRResNet (train: clean)	0.7569	0.7531	0.7274	0.6789	0.5828	0.5452	0.5149	0.4912	0.4729	0.4589	0.4481	0.4396	0.4329	0.4276	0.4232	0.4196	
SRResNet (train: blur0.4)	0.7495	0.7482	0.7425	0.7396	0.7357	0.7266	0.7063	0.6640	0.6043	0.5448	0.4990	0.4684	0.4487	0.4364	0.4286	0.4229	0.4185
SRResNet (train: blur2)	0.4559	0.4804	0.5755	0.7022	0.7497	0.6745	0.6024	0.5520	0.5161	0.4900	0.4709	0.4567	0.4458	0.4373	0.4307	0.4253	0.4210
SRResNet (train: blur0.4+noise0.20)	0.7377	0.7364	0.7288	0.7234	0.7215	0.7103	0.6894	0.6553	0.6002	0.5430	0.5013	0.4724	0.4525	0.4385	0.4283	0.4208	0.4150
IKC	0.7583	0.7585	0.7494	0.7331	0.7231	0.7102	0.6895	0.6509	0.6018	0.5477	0.4992	0.4677	0.4488	0.4365	0.4275	0.4209	0.4157
DAN	0.7629	0.7616	0.7581	0.7556	0.7477	0.7251	0.6765	0.6084	0.5471	0.5061	0.4802	0.4623	0.4491	0.4393	0.4321	0.4264	0.4218
DASR	0.7559	0.7548	0.7515	0.7485	0.7425	0.7294	0.7024	0.6596	0.6027	0.5418	0.4986	0.4700	0.4513	0.4388	0.4300	0.4237	0.4184
Real-ESRGAN	0.6271	0.6268	0.6254	0.6219	0.6151	0.6042	0.5876	0.5635	0.5371	0.5186	0.5088	0.5063	0.5049	0.5021	0.4968	0.4910	0.4853
Real-ESRNet	0.6795	0.6792	0.6781	0.6750	0.6684	0.6563	0.6390	0.6157	0.5891	0.5660	0.5053	0.5449	0.5464	0.5442	0.5358	0.5266	0.5178
BSRGAN	0.6321	0.6320	0.6306	0.6264	0.6180	0.6055	0.5899	0.5725	0.5549	0.5366	0.5193	0.5038	0.4898	0.4771	0.4661	0.4567	0.4487
BSRNet	0.6814	0.6810	0.6788	0.6734	0.6636	0.6493	0.6314	0.6108	0.5878	0.5690	0.5446	0.5278	0.5139	0.5025	0.4935	0.4868	0.4817
SwinIR-GAN	0.6321	0.6317	0.6289	0.6226	0.6118	0.5965	0.5797	0.5377	0.5189	0.5007	0.4837	0.4673	0.4532	0.4420	0.4337	0.4277	
SwinIR-PSNR	0.6922	0.6917	0.6890	0.6831	0.6728	0.6579	0.6396	0.6192	0.5979	0.5770	0.5578	0.5407	0.5257	0.5153	0.5096	0.5060	0.5038

Table 10. Model performance (SSIM) on PIES-Blur dataset. Higher SSIM value denotes that the output images are structurally closer to the ground truth images.

Methods	Clean	Blur Level															
		0.5	1.0	1.5	2.0	2.5	3.0	3.5	4.0	4.5	5.0	5.5	6.0	6.5	7.0	7.5	8.0
SRResNet (train: clean)	0.2136	0.2216	0.2669	0.3511	0.4339	0.4979	0.5476	0.5860	0.6150	0.6359	0.6503	0.6601	0.6666	0.6709	0.6738	0.6758	0.6770
SRResNet (train: blur0.4)	0.2202	0.2233	0.2320	0.2324	0.2345	0.2436	0.2666	0.3234	0.4173	0.5154	0.5738	0.5957	0.6062	0.6141	0.6207	0.6248	0.6267
SRResNet (train: blur2)	0.3379	0.3217	0.2669	0.2130	0.2186	0.3487	0.4637	0.5336	0.5811	0.6135	0.6343	0.6470	0.6543	0.6582	0.6597	0.6600	0.6592
SRResNet (train: blur0.4+noise0.20)	0.2299	0.2337	0.2471	0.2503	0.2464	0.2594	0.2891	0.3363	0.4160	0.5073	0.5688	0.5968	0.6078	0.6109	0.6103	0.6088	0.6066
IKC	0.2058	0.2100	0.2321	0.2564	0.2693	0.2837	0.3016	0.3442	0.4003	0.4719	0.5287	0.5530	0.5646	0.5681	0.5674	0.5658	0.5633
DAN	0.2042	0.2086	0.2178	0.2220	0.2334	0.2670	0.3418	0.4454	0.5344	0.5900	0.6194	0.6357	0.6457	0.6507	0.6526	0.6531	0.6518
DASR	0.2138	0.2169	0.2229	0.2262	0.2326	0.2471	0.2797	0.3346	0.4159	0.5077	0.5583	0.5802	0.5866	0.5881	0.5893	0.5889	0.5885
Real-ESRGAN	0.1932	0.1935	0.1948	0.1975	0.2027	0.2115	0.2249	0.2418	0.2601	0.2759	0.2880	0.2953	0.2969	0.2973	0.2996	0.3022	0.3052
Real-ESRNet	0.2843	0.2851	0.2881	0.2932	0.3020	0.3161	0.3361	0.3865	0.4104	0.4268	0.4315	0.4255	0.4194	0.4194	0.4227	0.4270	
BSRGAN	0.1909	0.1910	0.1918	0.1949	0.2010	0.2104	0.2230	0.2390	0.2576	0.2781	0.2983	0.3160	0.3309	0.3427	0.3519	0.3588	0.3632
BSRNet	0.2790	0.2800	0.2841	0.2917	0.3040	0.3206	0.3414	0.3661	0.3945	0.4237	0.4494	0.4706	0.4880	0.5018	0.5111	0.5162	0.5184
SwinIR-GAN	0.1724	0.1728	0.1742	0.1778	0.1845	0.1947	0.2083	0.2228	0.2379	0.2527	0.2670	0.2806	0.2906	0.2987	0.3041	0.3076	0.3102
SwinIR-PSNR	0.2671	0.2683	0.2724	0.2792	0.2897	0.3047	0.3234	0.3444	0.3667	0.3889	0.4092	0.4270	0.4413	0.4505	0.4547	0.4568	0.4580

Table 11. Model performance (LPIPS) on PIES-Blur dataset. Lower LPIPS value denotes that the output images are perceptually closer to the ground truth images.

Methods	Clean	Blur Level															
		0.5	1.0	1.5	2.0	2.5	3.0	3.5	4.0	4.5	5.0	5.5	6.0	6.5	7.0	7.5	8.0
SRResNet (train: clean)	12.28	12.39	13.64	14.84	14.90	14.52	14.73	15.03	15.34	15.68	16.01	16.28	16.54	16.71	16.84	16.91	16.98
SRResNet (train: blur0.4)	12.20	12.31	12.67	12.69	12.67	13.00	13.13	14.09	17.64	15.72	14.84	14.59	14.68	14.76	14.95	14.98	15.01
SRResNet (train: blur2)	26.71	24.98	18.47	13.48	12.44	15.15	14.82	14.63	14.82	15.05	15.33	15.59	15.79	15.92	15.99	16.01	16.00
SRResNet (train: blur0.4+noise0.20)	12.76	12.82	13.03	12.95	12.91	13.09	13.62	15.30	18.42	19.59	16.96	15.49	15.62	15.44	14.70	14.63	14.57
IKC	13.11	13.20	13.65	14.40	13.96	13.98	14.32	14.66	13.98	14.10	14.51	14.86	14.81	14.79	14.71	14.68	14.65
DAN	12.09	12.20	12.39	12.40	12.66	13.47	14.17	14.78	14.49	14.90	15.21	15.60	15.95	16.15	16.24	16.29	16.26
DASR	11.64	11.80	12.05	12.15	12.41	12.78	13.64	14.48	14.71	13.69	13.60	13.83	13.94	14.13	14.06	14.22	14.27
Real-ESRGAN	10.15	10.14	10.12	10.10	10.14	10.18	10.22	11.05	10.98	10.64	11.18	11.00	10.35	10.31	10.33	10.37	10.48
Real-ESRNet	13.76	13.80	13.87	13.95	14.16	14.12	14.35	16.30	16.06	16.58	16.84	16.97	17.07	17.10	17.61	18.12	18.36
BSRGAN	9.77	9.77	9.76	9.72	9.75	9.80	9.81	9.97	10.16	10.30	10.52	10.63	10.74	10.73	10.78	10.64	10.51
BSRNet	14.11	14.15	14.38	14.64	14.98	15.35	15.90	16.60	17.72	19.28	20.25	20.00	19.59	18.86	18.50	18.36	18.28
SwinIR-GAN	9.83	9.83	9.84	9.91	9.89	9.94	10.05	10.17	10.08	10.11	10.10	10.18	10.07	10.15	10.16	10.22	10.24
SwinIR-PSNR	13.48	13.55	13.75	13.97	14.18	14.44	14.75	15.13	15.48	15.80	16.15	16.47	16.53	16.75	16.88	16.95	16.80

Table 12. Model performance (NIQE) on PIES-Blur dataset. Lower NIQE value denotes better perceptual quality.

Methods	Clean	Noise Level									
		5	10	15	20	25	30	35	40	45	50
SRResNet (train: clean)	25.87	23.92	21.66	19.66	17.95	16.52	15.35	14.39	13.61	12.96	12.42
SRResNet (train: noise0_20)	25.59	25.02	24.32	23.67	23.11	22.47	20.94	18.62	16.70	15.30	14.27
SRResNet (train: blur0_4+noise0.20)	25.10	24.64	24.04	23.45	22.94	22.32	21.47	20.52	19.68	19.02	18.56
Real-ESRGAN	21.90	21.81	21.45	20.95	20.49	20.06	19.64	19.26	18.93	18.63	18.38
Real-ESRNet	23.41	23.31	22.87	22.32	21.81	21.35	20.90	20.45	20.04	19.58	19.17
BSRGAN	22.54	22.14	21.16	19.94	18.77	17.72	16.81	16.01	15.35	14.75	14.20
BSRNet	23.79	23.32	22.18	20.95	19.80	18.78	17.95	17.28	16.73	16.26	15.83
SwinIR-GAN	22.06	21.84	21.27	20.63	20.01	19.47	18.96	18.52	18.09	17.76	17.42
SwinIR-PSNR	23.62	23.40	22.75	22.00	21.24	20.47	19.71	19.00	18.31	17.72	17.13

Table 13. Model performance (PSNR) on PIES-Noise dataset. Higher PSNR value denotes that the output images are closer to the ground truth images in content.

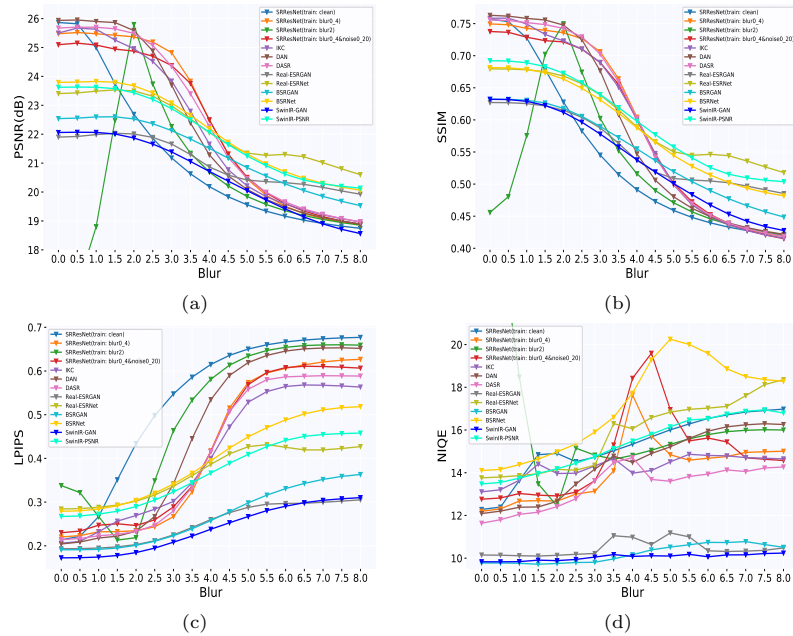


Fig. 9. The PSNR, SSIM, LPIPS and NIQE curves of different methods on PIES-Blur dataset.

Methods	Clean	Noise Level									
		5	10	15	20	25	30	35	40	45	50
SRRResNet (train: clean)	0.7569	0.6394	0.4964	0.3920	0.3173	0.2635	0.2242	0.1948	0.1729	0.1550	0.1409
SRRResNet (train: noise0.20)	0.7473	0.7199	0.6876	0.6593	0.6357	0.6130	0.5379	0.4223	0.3317	0.2661	0.2199
SRRResNet (train: blur_0.4+noise0.20)	0.7377	0.7159	0.6873	0.6613	0.6399	0.6149	0.5724	0.5225	0.4780	0.4434	0.4209
Real-ESRGAN	0.6271	0.6140	0.5899	0.5649	0.5419	0.5245	0.5065	0.4898	0.4760	0.4633	0.4512
Real-ESRNet	0.6795	0.6668	0.6402	0.6135	0.5891	0.5699	0.5518	0.5344	0.5212	0.5069	0.4934
BSRGAN	0.6321	0.6076	0.5640	0.5151	0.4666	0.4220	0.3828	0.3494	0.3222	0.2996	0.2801
BSRNet	0.6814	0.6573	0.6122	0.5657	0.5225	0.4860	0.4549	0.4286	0.4076	0.3903	0.3750
SwinIR-GAN	0.6321	0.6137	0.5792	0.5455	0.5162	0.4909	0.4664	0.4432	0.4206	0.4022	0.3823
SwinIR-PSNR	0.6922	0.6752	0.6393	0.6050	0.5741	0.5462	0.5187	0.4935	0.4698	0.4487	0.4271

Table 14. Model performance (SSIM) on PIES-Noise dataset. Higher SSIM value denotes that the output images are structurally closer to the ground truth images.

Methods	Clean	Noise Level									
		5	10	15	20	25	30	35	40	45	50
SRResNet (train: clean)	0.2136	0.3226	0.4664	0.5602	0.6133	0.6482	0.6710	0.6888	0.7032	0.7159	0.7267
SRResNet (train: noise0_20)	0.2184	0.2391	0.2648	0.2870	0.3048	0.3080	0.3636	0.4646	0.5372	0.5877	0.6236
SRResNet (train: blur0_4+noise0_20)	0.2299	0.2441	0.2709	0.2961	0.3155	0.3231	0.3418	0.3649	0.3877	0.4059	0.4199
Real-ESRGAN	0.1932	0.1974	0.2117	0.2300	0.2466	0.2648	0.2825	0.3008	0.3173	0.3329	0.3496
Real-ESRNet	0.2843	0.2938	0.3158	0.3390	0.3587	0.3752	0.3892	0.4013	0.4125	0.4213	0.4288
BSRGAN	0.1909	0.1995	0.2279	0.2657	0.3020	0.3314	0.3576	0.3820	0.4036	0.4246	0.4434
BSRNet	0.2790	0.2907	0.3203	0.3524	0.3830	0.4079	0.4304	0.4509	0.4696	0.4875	0.5019
DASR-N-Ani	0.2248	0.2429	0.2674	0.2937	0.3149	0.3301	0.3371	0.3519	0.3797	0.4057	0.4293
SwinIR-GAN	0.1724	0.1779	0.2009	0.2309	0.2566	0.2777	0.2925	0.3116	0.3261	0.3401	0.3570
SwinIR-PSNR	0.2671	0.2759	0.3049	0.3320	0.3538	0.3722	0.3879	0.4013	0.4142	0.4225	0.4333

Table 15. Model performance (LPIPS) on PIES-Noise dataset. Lower LPIPS value denotes that the output images are perceptually closer to the ground truth images.

Methods	Clean	Noise Level									
		5	10	15	20	25	30	35	40	45	50
SRResNet (train: clean)	12.28	13.07	13.25	13.38	13.52	13.71	14.14	14.36	14.84	15.36	16.08
SRResNet (train: noise0_20)	12.54	12.95	13.08	13.33	13.37	12.49	12.04	13.39	15.41	16.63	17.65
SRResNet (train: blur0_4+noise0_20)	12.76	13.05	13.23	13.64	13.84	14.03	14.58	14.78	15.00	14.78	13.94
Real-ESRGAN	10.15	10.16	10.31	10.48	10.61	10.74	10.72	10.76	10.88	10.86	11.07
Real-ESRNet	13.76	13.76	13.98	14.32	14.39	14.28	14.30	14.05	13.99	13.62	13.25
BSRGAN	9.77	9.88	10.02	10.45	10.79	11.11	11.55	11.85	12.70	13.05	12.60
BSRNet	14.11	13.99	14.26	14.65	14.78	14.79	14.83	14.86	14.76	14.81	14.33
DASR-N-Ani	12.12	12.68	13.14	14.01	14.34	14.38	14.10	14.23	14.10	14.04	13.74
SwinIR-GAN	9.83	9.82	9.84	9.93	9.79	9.59	9.38	9.14	8.95	8.77	8.67
SwinIR-PSNR	13.48	13.49	13.86	13.94	13.83	13.52	13.35	12.86	12.46	12.08	11.70

Table 16. Model performance (NIQE) on PIES-Noise dataset. Lower NIQE value denotes better perceptual quality.

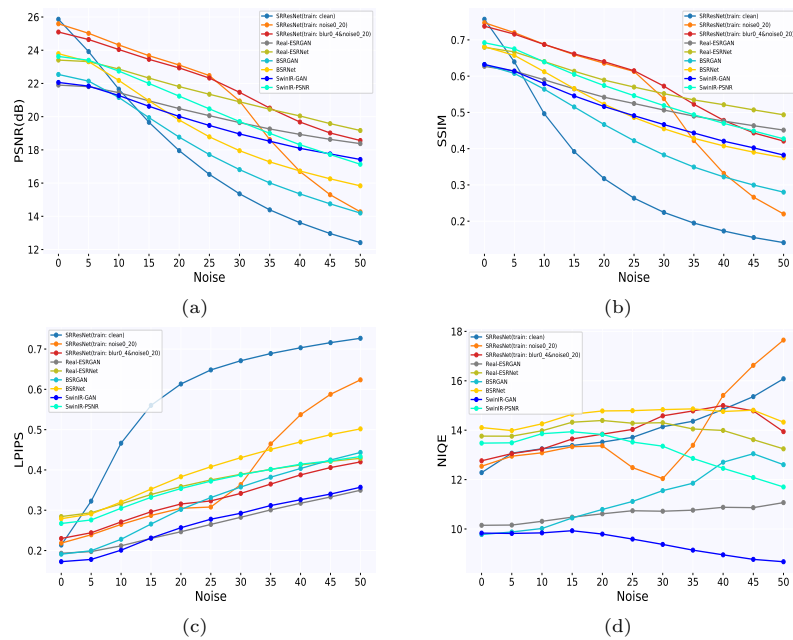


Fig. 10. The PSNR, SSIM, LPIPS and NIQE curves of different methods on PIES-Noise dataset.

Methods	Blur1			Blur2			Blur4			Blur6			
	clean	n10	n20	n30									
SRResNet(train: clean)	25.87	21.50	17.93	15.32	20.58	17.55	15.09	18.91	16.61	14.48	18.13	16.11	14.14
SRResNet (train: blur0_4)	25.48	21.68	18.12	15.66	20.74	17.73	15.40	19.03	16.77	14.75	18.23	16.25	14.39
SRResNet (train: noise0_20)	25.59	23.88	22.80	20.85	22.12	21.56	20.18	19.91	19.65	18.72	19.01	18.83	18.01
SRResNet (train: blur0_4+noise0_20)	25.10	23.90	22.75	21.48	23.14	22.10	20.98	21.38	20.47	19.39	19.55	19.18	18.56
Real-ESRGAN	21.90	21.45	20.45	19.60	21.25	20.22	19.38	20.12	19.31	18.78	19.33	18.76	18.37
Real-ESRNet	23.41	22.82	21.72	20.81	22.49	21.36	20.48	21.00	20.15	19.53	20.08	19.43	18.92
BSRGAN	22.54	21.13	18.72	16.73	20.93	18.52	16.57	19.99	17.78	16.06	19.20	17.30	15.75
BSRNet	23.79	22.11	19.71	17.87	21.79	19.43	17.68	20.64	18.61	17.13	19.74	18.08	16.79
SwinIR-GAN	22.06	21.20	19.91	18.83	20.81	19.51	18.46	19.49	18.34	17.45	18.44	17.55	16.92
SwinIR-PSNR	23.62	22.63	21.11	19.58	22.19	20.68	19.23	20.78	19.50	18.28	19.77	18.78	17.72

Table 17. Model performance (PSNR) on PIES-BlurNoise dataset. Higher PSNR value denotes that the output images are closer to the ground truth images in content. n10 represents noise level 10.

Methods	Blur1			Blur2			Blur4			Blur6			
	clean	n10	n20	n30									
SRResNet (train: clean)	0.7569	0.4762	0.3020	0.2110	0.4122	0.2574	0.1779	0.3087	0.1839	0.1235	0.2698	0.1557	0.1032
SRResNet (train: blur0.4)	0.7495	0.4926	0.3160	0.2256	0.4286	0.2709	0.1909	0.3233	0.1949	0.1337	0.2834	0.1655	0.1120
SRResNet (train: noise0_20)	0.7473	0.6623	0.6144	0.5227	0.5821	0.5524	0.4744	0.4718	0.4591	0.3859	0.4313	0.4237	0.3484
SRResNet (train: blur0.4+noise0.20)	0.7377	0.6719	0.6238	0.5630	0.6327	0.5853	0.5257	0.5388	0.4992	0.4374	0.4546	0.4411	0.3979
Real-ESRGAN	0.6271	0.5834	0.5346	0.4991	0.5605	0.5124	0.4781	0.4925	0.4565	0.4364	0.4517	0.4284	0.4149
Real-ESRNet	0.6795	0.6323	0.5795	0.5418	0.6060	0.5523	0.5159	0.5285	0.4889	0.4633	0.4856	0.4569	0.4359
BSRGAN	0.6321	0.5583	0.4611	0.3773	0.5382	0.4419	0.3637	0.4769	0.3968	0.3324	0.4352	0.3719	0.3163
BSRNet	0.6814	0.6047	0.5143	0.4478	0.5808	0.4927	0.4316	0.5134	0.4436	0.3966	0.4676	0.4160	0.3789
SwinIR-GAN	0.6321	0.5722	0.5082	0.4564	0.5436	0.4828	0.4342	0.4714	0.4225	0.3809	0.4214	0.3844	0.3535
SwinIR-PSNR	0.6922	0.6305	0.5642	0.5085	0.6015	0.5369	0.4839	0.5305	0.4768	0.4324	0.4870	0.4442	0.4060

Table 18. Model performance (SSIM) on PIES-BlurNoise dataset. Higher SSIM value denotes that the output images are structurally closer to the ground truth images.

Methods	clean	Blur1			Blur2			Blur4			Blur6		
		n10	n20	n30									
SRResNet (train: clean)	0.2136	0.5064	0.6379	0.6815	0.5853	0.6773	0.7000	0.6587	0.7054	0.7092	0.6741	0.7093	0.7097
SRResNet (train: blur0.4)	0.2202	0.4911	0.6363	0.6858	0.5705	0.6761	0.7058	0.6508	0.7078	0.7181	0.6674	0.7133	0.7176
SRResNet (train: noise0.20)	0.2184	0.3043	0.3384	0.3842	0.4369	0.4397	0.4410	0.6027	0.5888	0.5157	0.6530	0.6388	0.5344
SRResNet (train: blur0.4+noise0.20)	0.2299	0.2944	0.3396	0.3564	0.3420	0.3883	0.4009	0.4691	0.5149	0.4886	0.6088	0.6092	0.5184
Real-ESRGAN	0.1932	0.2175	0.2572	0.2937	0.2360	0.2798	0.3224	0.3080	0.3604	0.4100	0.3623	0.4240	0.4818
Real-ESRNet	0.2843	0.3268	0.3729	0.4037	0.3599	0.4088	0.4409	0.4505	0.4901	0.5202	0.5049	0.5379	0.5666
BSRGAN	0.1909	0.2329	0.3071	0.3647	0.2506	0.3266	0.3822	0.3127	0.3816	0.4257	0.3668	0.4163	0.4538
BSRNet	0.2790	0.3303	0.3945	0.4414	0.3601	0.4242	0.4667	0.4490	0.4942	0.5249	0.5155	0.5349	0.5566
SwinIR-GAN	0.1724	0.2080	0.2654	0.3031	0.2305	0.2855	0.3220	0.2870	0.3318	0.3674	0.3218	0.3610	0.3919
SwinIR-PSNR	0.2671	0.3158	0.3684	0.4027	0.3476	0.4004	0.4366	0.4243	0.4685	0.5036	0.4718	0.5072	0.5371

Table 19. Model performance (LPIPS) on PIES-BlurNoise dataset. Lower LPIPS value denotes that the output images are perceptually closer to the ground truth images.

Methods	clean	Blur1			Blur2			Blur4			Blur6		
		n10	n20	n30									
SRResNet (train: clean)	12.28	12.21	12.23	13.18	8.86	10.30	11.80	7.45	9.86	11.80	7.54	10.26	12.24
SRResNet (train: blur0.4)	12.20	11.91	12.06	12.68	8.80	10.27	11.56	7.17	9.65	11.60	7.22	10.10	12.04
SRResNet (train: noise0.20)	12.54	13.80	13.91	11.98	15.93	16.64	11.87	15.65	15.52	9.31	16.36	15.84	9.21
SRResNet (train: blur0.4+noise0.20)	12.76	13.60	14.14	13.95	14.38	14.70	13.21	17.03	18.15	10.72	16.73	15.68	10.32
Real-ESRGAN	10.15	10.24	10.73	10.83	10.30	10.57	10.76	10.94	11.46	11.37	11.05	11.36	12.11
Real-ESRNet	13.76	14.31	14.83	14.56	14.83	15.26	15.26	17.68	16.95	15.92	18.28	17.14	17.08
BSRGAN	9.77	10.05	10.86	11.70	10.10	10.78	11.78	10.93	11.13	11.81	10.59	11.13	11.94
BSRNet	14.11	14.57	15.25	15.15	15.16	15.76	15.71	18.58	17.13	17.22	19.37	19.62	18.58
SwinIR-GAN	9.83	10.00	10.06	9.36	10.09	9.84	9.39	10.17	9.72	9.19	10.05	9.83	9.14
SwinIR-PSNR	13.48	14.14	14.14	13.50	14.66	14.75	14.13	16.09	16.03	14.92	17.03	16.58	16.18

Table 20. Model performance (NIQE) on PIES-BlurNoise dataset. Lower NIQE value denotes better perceptual quality.

Methods	PIES800-RealCam			PIES800-RealLQ		
	n10	n20	n30	n10	n20	n30
SRResNet (train: clean)	22.40			14.40		
SRResNet (train: blur0.4)	22.40			14.03		
SRResNet (train: noise0.20)	23.71			15.67		
SRResNet (train: blur0.4+noise0.20)	23.63			14.02		
IKC	21.60			13.77		
DAN	22.86			14.00		
DASR	22.74			13.44		
Real-ESRGAN	18.94			13.53		
Real-ESRNet	26.86			18.02		
BSRGAN	20.30			13.09		
BSRNet	32.71			18.39		
SwinIR-GAN	17.75			12.84		
SwinIR-PSNR	27.82			17.78		

Table 21. Model performance (NIQE) on PIES-RealCam and PIES-RealLQ datasets. Lower NIQE value denotes better perceptual quality.

Methods	Clean	Blur Level																
		0.5	1.0	1.5	2.0	2.5	3.0	3.5	4.0	4.5	5.0	5.5	6.0	6.5	7.0	7.5	8.0	
SRResNet (train: clean)	σ	2.718	2.668	2.532	2.418	2.333	2.260	2.194	2.138	2.083	2.042	2.007	1.983	1.965	1.948	1.933	1.920	1.911
	α	0.687	0.684	0.661	0.628	0.596	0.568	0.539	0.514	0.494	0.478	0.466	0.454	0.446	0.440	0.436	0.432	0.428
SRResNet (train: blur0.4)	σ	2.866	2.840	2.783	2.787	2.795	2.785	2.735	2.599	2.465	2.370	2.299	2.245	2.203	2.170	2.142	2.122	2.101
	α	0.691	0.686	0.682	0.683	0.683	0.682	0.667	0.632	0.591	0.555	0.526	0.505	0.489	0.478	0.468	0.461	0.457
IKC	σ	1.291	1.245	1.133	1.062	1.048	1.049	1.068	1.082	1.100	1.066	0.977	0.895	0.834	0.800	0.781	0.768	0.760
	α	0.770	0.774	0.778	0.774	0.779	0.786	0.798	0.795	0.787	0.764	0.718	0.678	0.643	0.619	0.604	0.595	0.588
DAN	σ	4.278	4.152	4.025	3.986	3.849	3.610	3.273	2.902	2.669	2.542	2.465	2.404	2.357	2.317	2.291	2.276	2.264
	α	0.668	0.675	0.673	0.680	0.690	0.695	0.689	0.660	0.605	0.559	0.529	0.506	0.488	0.474	0.463	0.456	0.452
RealESRGAN	σ	5.022	5.007	4.952	4.879	4.794	4.728	4.645	4.575	4.513	4.452	4.393	4.348	4.312	4.270	4.248	4.234	4.230
	α	0.790	0.788	0.784	0.781	0.781	0.775	0.778	0.776	0.776	0.772	0.768	0.761	0.758	0.757	0.755	0.750	0.747
RealESRNet	σ	3.718	3.707	3.678	3.645	3.613	3.579	3.562	3.350	3.512	3.462	3.421	3.351	3.269	3.251	3.233	3.213	3.197
	α	0.739	0.739	0.738	0.734	0.725	0.721	0.717	0.708	0.699	0.683	0.673	0.659	0.656	0.657	0.661	0.663	0.662
BSRGAN	σ	8.921	8.900	8.814	8.689	8.531	8.360	8.183	8.026	7.888	7.781	7.695	7.615	7.553	7.493	7.456	7.409	7.373
	α	0.762	0.762	0.760	0.756	0.749	0.744	0.737	0.726	0.720	0.710	0.701	0.694	0.685	0.678	0.671	0.668	0.662
BSRNet	σ	5.339	5.328	5.289	5.234	5.165	5.092	5.015	4.939	4.857	4.788	4.734	4.678	4.631	4.584	4.552	4.527	4.510
	α	0.693	0.693	0.689	0.684	0.677	0.668	0.659	0.647	0.635	0.622	0.608	0.594	0.581	0.571	0.562	0.557	0.554
DASR	σ	6.416	6.293	6.107	6.058	5.948	5.747	5.445	5.087	4.691	4.342	4.155	4.020	3.908	3.837	3.773	3.747	3.713
	α	0.679	0.682	0.683	0.686	0.693	0.705	0.715	0.727	0.704	0.649	0.603	0.571	0.551	0.537	0.524	0.518	0.513
SRResNet (train: blur0.4+noise0.20)	σ	3.171	3.137	3.064	3.059	3.100	3.084	3.020	2.893	2.735	2.612	2.529	2.477	2.435	2.406	2.380	2.358	2.342
	α	0.696	0.694	0.682	0.683	0.689	0.687	0.678	0.646	0.595	0.552	0.521	0.500	0.486	0.475	0.469	0.463	0.459
SwinIR-GAN	σ	5.178	5.164	5.140	5.110	5.069	5.036	5.002	4.965	4.929	4.903	4.886	4.884	4.891	4.906	4.926	4.941	4.953
	α	0.740	0.742	0.742	0.742	0.742	0.736	0.734	0.732	0.733	0.736	0.738	0.739	0.735	0.733	0.734	0.735	
SwinIR-PSNR	σ	4.279	4.275	4.267	4.254	4.239	4.218	4.184	4.145	4.107	4.067	4.046	4.025	3.997	3.983	3.987	3.986	3.991
	α	0.747	0.746	0.746	0.744	0.740	0.737	0.737	0.736	0.739	0.741	0.740	0.735	0.732	0.728	0.722	0.719	0.717

Table 22. The estimated GGD parameters σ and α of representative methods with different degraded input.

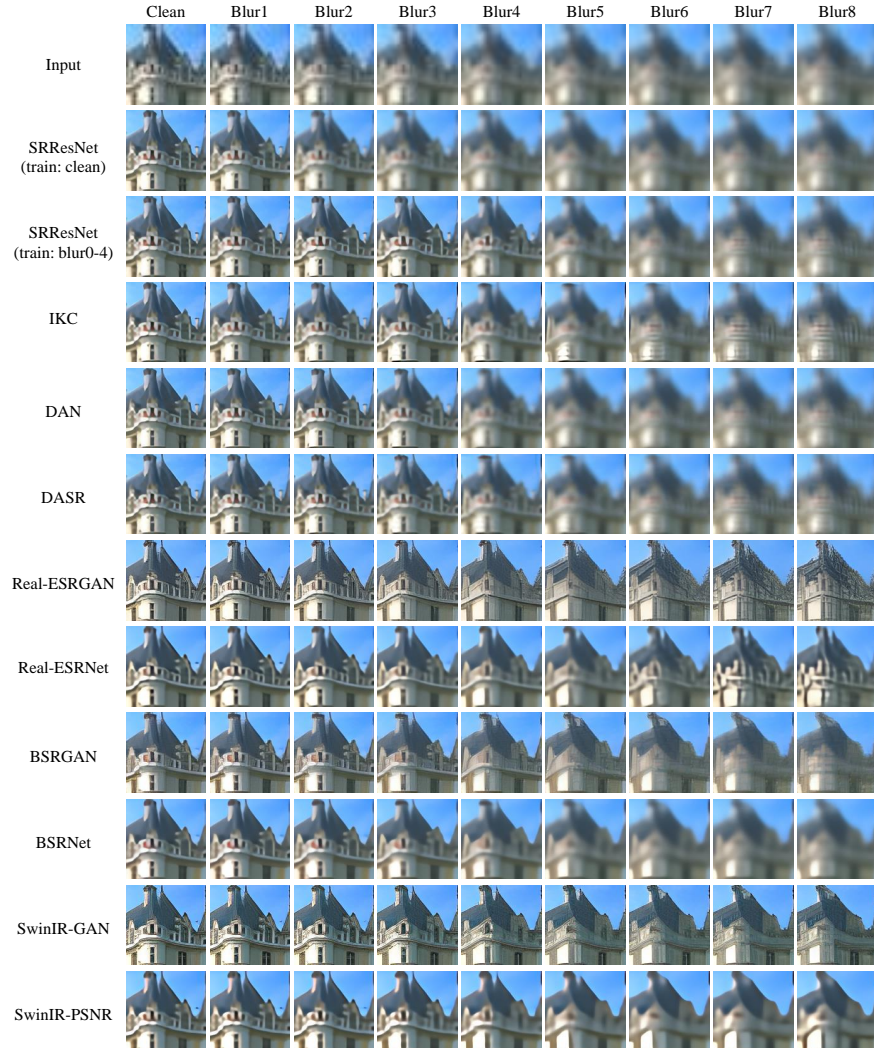


Fig. 11. Visual comparison on PIES-Blur dataset (1).

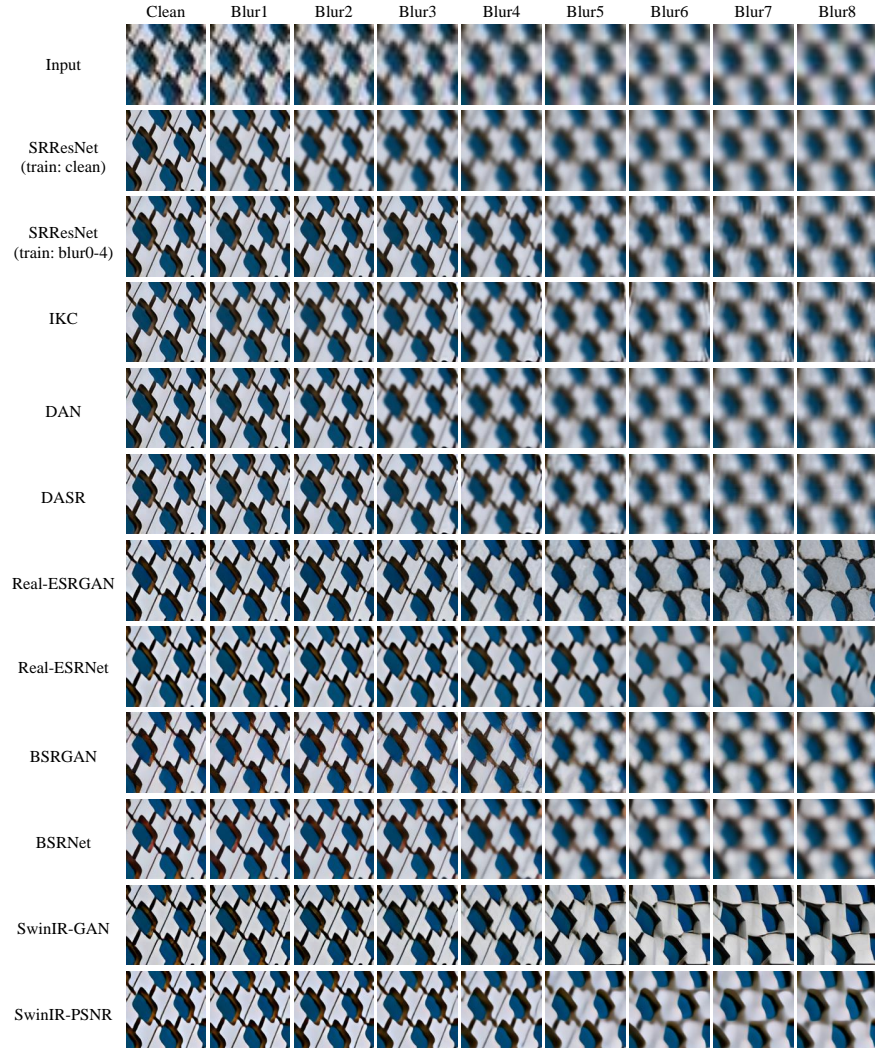


Fig. 12. Visual comparison on PIES-Blur dataset (2).

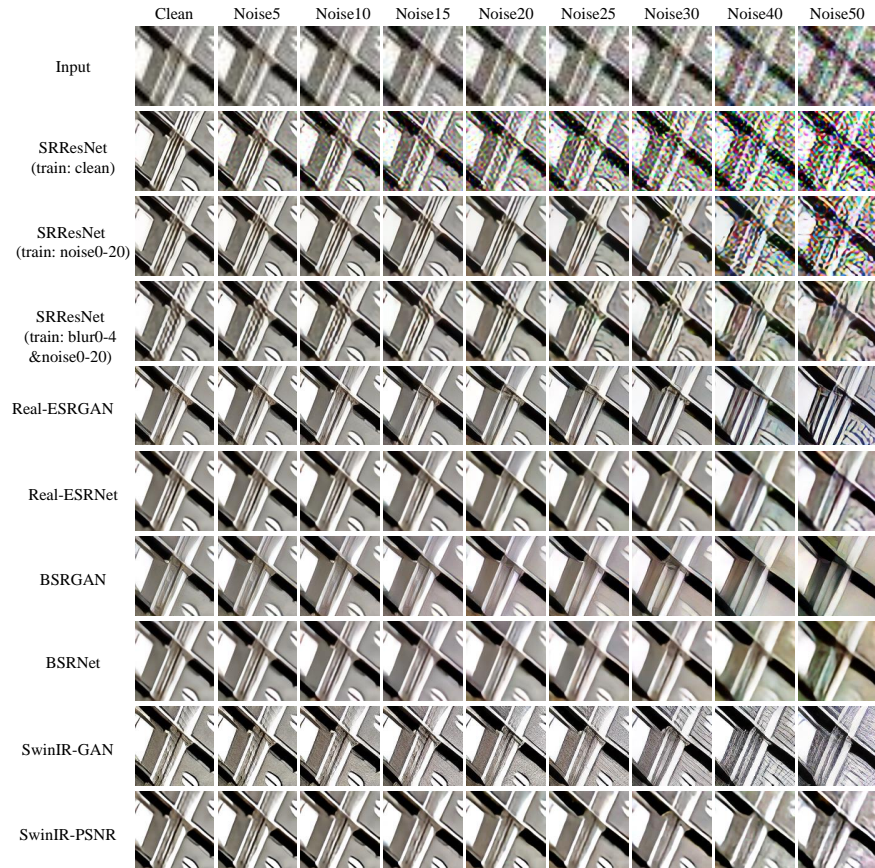


Fig. 13. Visual comparison on PIES-Noise dataset (1).

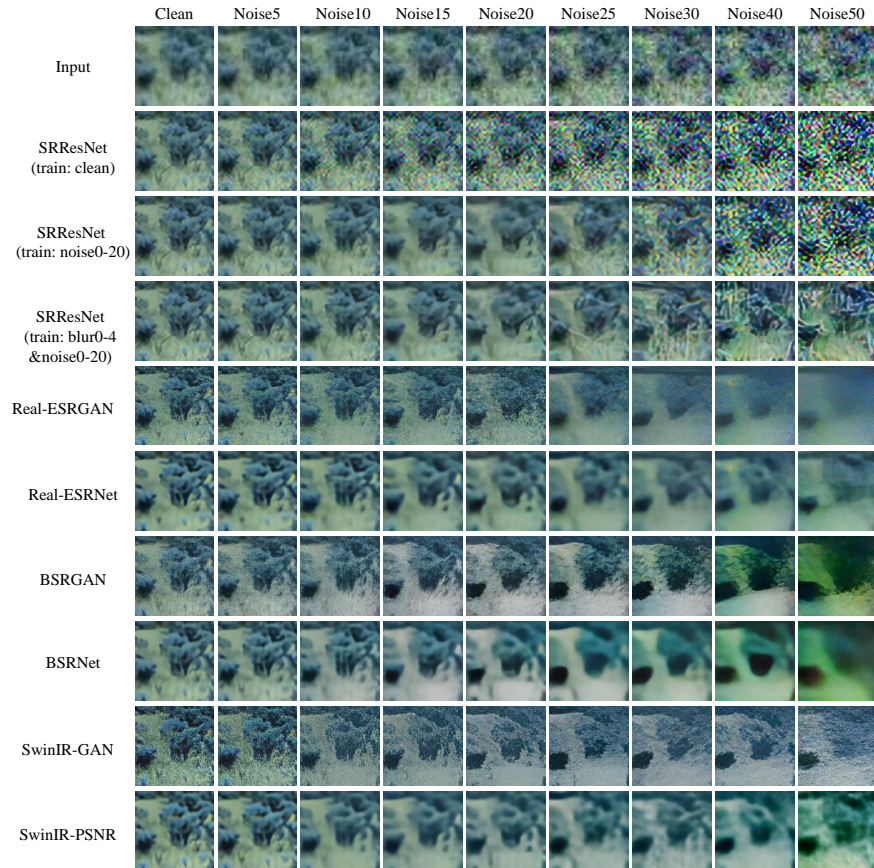


Fig. 14. Visual comparison on PIES-Noise dataset (2).

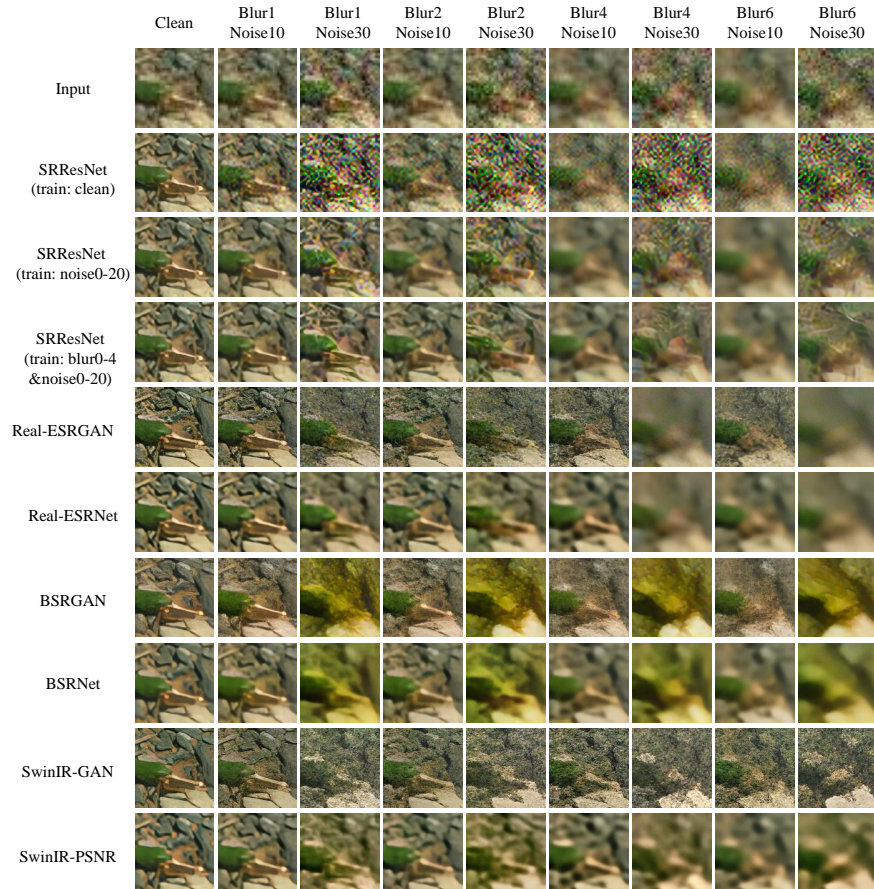


Fig. 15. Visual comparison on PIES-BlurNoise dataset.

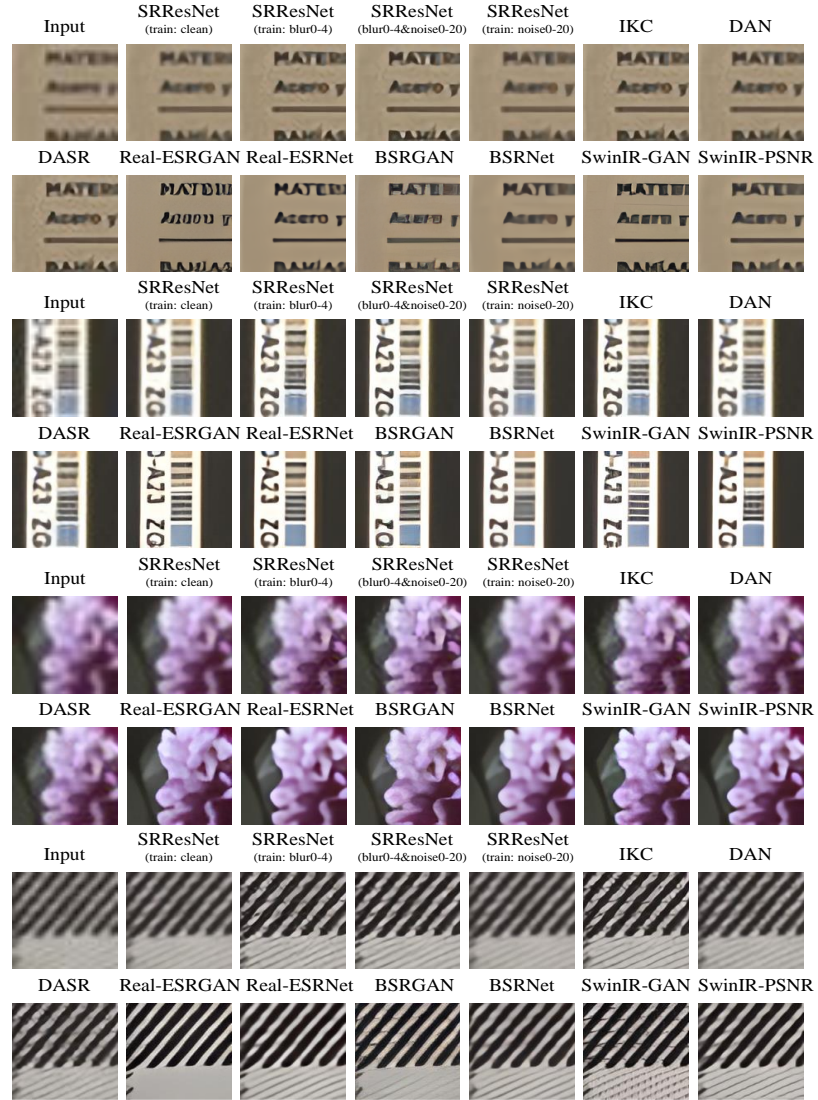


Fig. 16. Visual comparison on PIES-RealCam dataset.

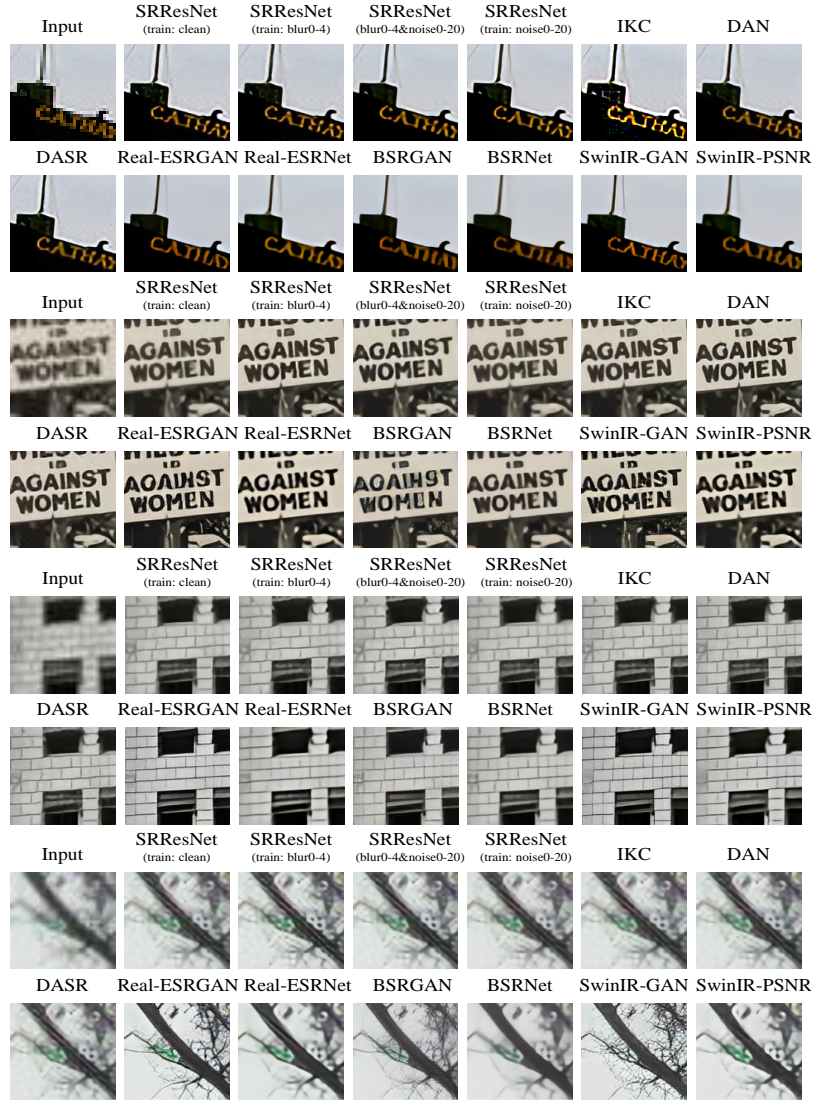


Fig. 17. Visual comparison on PIES-RealLQ dataset.

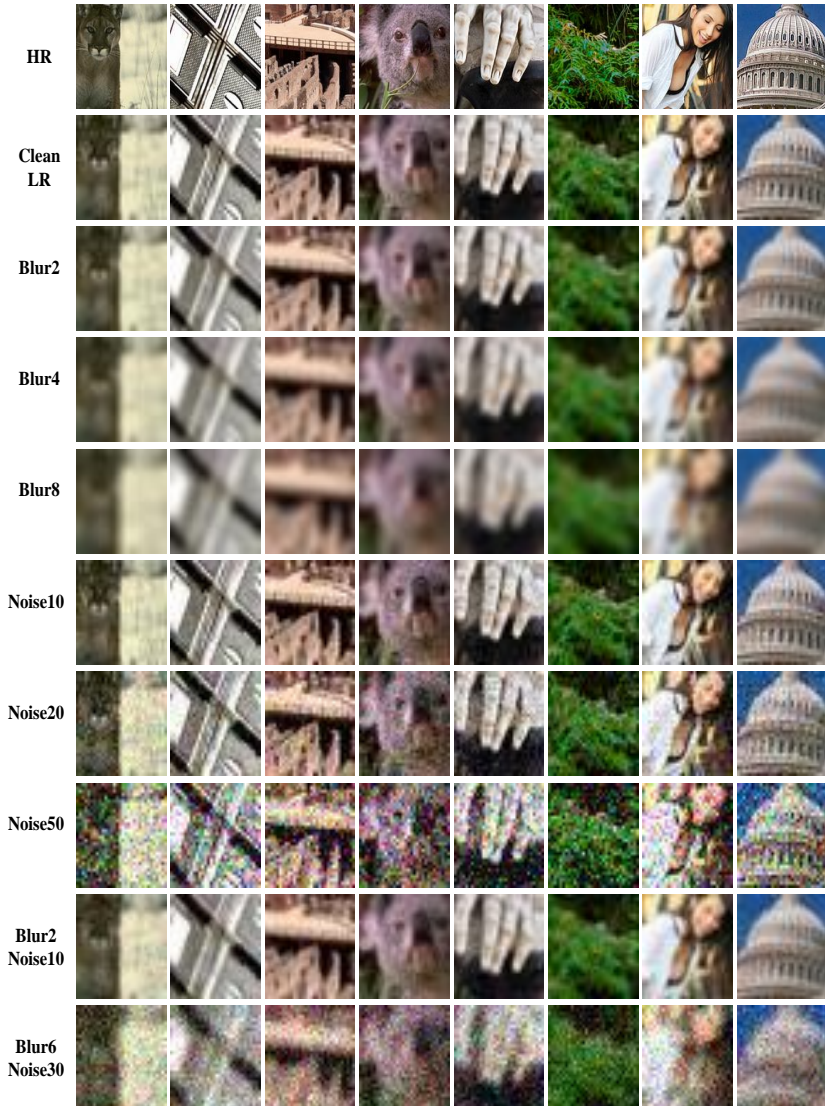


Fig. 18. Samples of PIES-Blur, PIES-Noise and PIES-BlurNoise datasets.

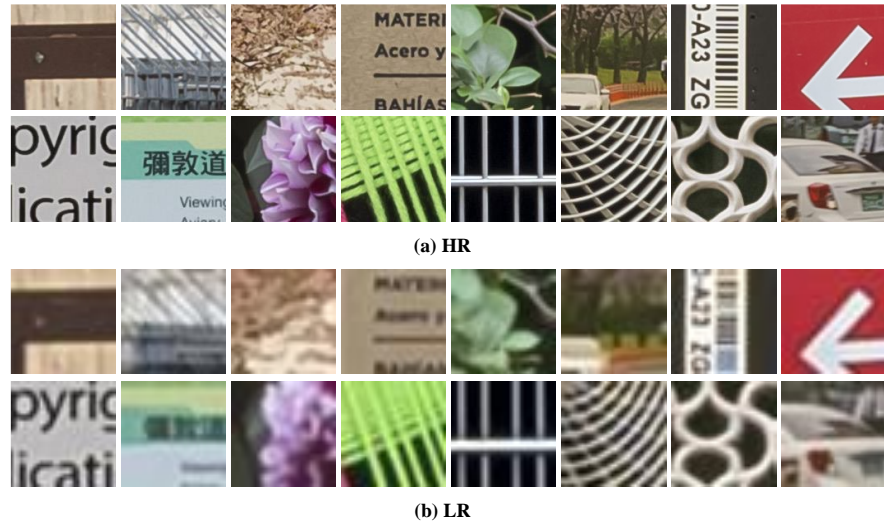


Fig. 19. Samples of PIES-RealCam dataset.



Fig. 20. Samples of PIES-RealLQ dataset.